**Biogeosciences
Discussions**

Modeling benthic-pelagic nutrient exchange processes and porewater distributions in a seasonally-hypoxic sediment: evidence for massive phosphate release by *Beggiatoa*?

A. W. Dale, V. J. Bertics, T. Treude, S. Sommer, and K. Wallmann

Helmholtz Centre for Ocean Research Kiel (GEOMAR), Wischhofstrasse 1–3,
24148 Kiel, Germany

Correspondence to: A. W. Dale (adale@geomar.de)

BGD

9, 11517–11575, 2012

Benthic fluxes in seasonally-hypoxic sediments

A. W. Dale et al.

Title Page

Abstract	Introduction
Conclusions	References
Tables	Figures

Back | Close

Full Screen / Esc

Printer-friendly Version

Interactive Discussion

Abstract

This study presents benthic data from 12 samplings from February to December 2010 in a 2 m deep channel in the southwest Baltic Sea. In winter, the distribution of solutes in the porewater was strongly modulated by bioirrigation which efficiently flushed the upper 1 cm of sediment, leading to concentrations which varied little from bottom water values. Solute pumping by bioirrigation fell sharply in summer as the bottom waters became severely hypoxic ($<2\,\mu M$ O_2). At this point the giant sulfide-oxidizing bacteria *Beggiatoa* was visible on surface sediments. Despite an increase in O_2 following mixing of the water column in November, macrofauna remained absent until the end of the sampling. Contrary to expectations, metabolites such as dissolved inorganic carbon, ammonium and hydrogen sulfide did not accumulate in the porewater during the hypoxic period when bioirrigation was absent, but instead tended toward bottom water values. This was taken as evidence for episodic bubbling of methane gas out of the sediment acting as an abiogenic irrigation process. Escaping bubble may provide a pathway for enhanced nutrient release to the bottom water and exacerbate the feedbacks with hypoxia. Subsurface dissolved phosphate (TPO_4) peaks in excess of $400\,\mu M$ developed in autumn resulting in a very large diffusive TPO_4 flux to the water column of $0.7 \pm 0.2\,\mathrm{mmol\,m^{-2}\,d^{-1}}$. The model was not able to simulate this TPO_4 source as release of iron-bound P (Fe–P) or organic P. As an alternative hypothesis, the TPO_4 peak was reproduced using new kinetic expressions that allow *Beggiatoa* to take up porewater TPO_4 and accumulate an intracellular P pool during periods with oxic bottom waters. TPO_4 is then released during hypoxia, as previous published results with sulfide-oxidizing bacteria indicate. The TPO_4 added to the porewater over the year by organic P and Fe–P is recycled though *Beggiatoa*, meaning that no additional source of TPO_4 is needed to explain the TPO_4 peak. Further experimental studies are needed to strengthen this conclusion and rule out Fe–P and organic P as candidate sources of ephemeral TPO_4 release. A measured C/P ratio of <20 for the diffusive flux at the sediment surface during hypoxia directly demonstrates preferential release of P

Full Screen / Esc

Printer-friendly Version

Interactive Discussion

relative to C under low oxygen bottom waters. Our results suggest that sulfide oxidizing bacteria act as phosphorus capacitors in systems with oscillating redox conditions, releasing massive amounts of TPO_4 in a short space of time and dramatically increasing the internal loading of TPO_4 in overlying waters.

1 Introduction

The Baltic Sea is a marginal brackish sea in Northern Europe consisting of deep and shallow basins interconnected by sills and channels. The only exchange with the ocean occurs via the Kattegat where saline water from the North Sea flows into the Baltic Sea underneath a fresher outgoing water mass. This results in a stratified water column in the central Baltic Sea with hypoxic (O_2 <62 µM) or even anoxic bottom waters existing in the deep water areas (Conley et al., 2002). Widespread increases in the surface area affected by seasonal and permanent hypoxia and eutrophication are of prime concern for policy making and environmental management strategies by Baltic Sea states (HELCOM, 2009).

Sediments underlying seasonally hypoxic waters are important sites of preferential nutrient regeneration to the water column (Conley and Johnstone, 1995; Cowan and Boynton, 1996; Rozan et al., 2002; Reed et al., 2011). These return fluxes are generally enhanced by bioturbation and bioirrigation; processes that describe the mixing of sediment and porewater by animals (Aller and Aller, 1998). Hypoxia generally decreases biodiversity and macrofaunal abundance (Levin et al., 2009), thus altering the processing of organic material in time and space. Yet, the change in depth and intensity of sediment mixing by animals at the community level is extremely complex to predict due to the huge variability in ecology and tolerance levels of animals to low oxygen (see reviews by Levin et al., 2009; Middelburg and Levin, 2009). Consequently, a key challenge in understanding the impacts of hypoxia in shallow or semi-enclosed aquatic ecosystems, such as the Baltic Sea, is to predict the response of the benthic compartment to decreasing levels of oxygen. Nonetheless, knowledge on the sensitivity of

sediments to periodic and episodic fluctuations in bottom water O_2 still remains very fragmentary. This is partly because there are very few time-series field observations in such settings (e.g. Rozan et al., 2002). Better incorporation of time-series benthic field data into models should greatly improve the predictive capacity of feedbacks operating between the sediment and water column in areas prone to hypoxia (e.g. Eilola et al., 2011).

Reduction of ferric oxyhydroxide phases and release of iron-bound P to the porewater during hypoxia has been proposed as a major source of phosphate to the overlying water column by some authors (e.g. Sundby et al., 1992; McManus et al., 1997). Other authors highlight the potential role of microorganisms (Ingall and Jahnke, 1997; Hupfer et al., 2004; Sannigrahi and Ingall, 2005). Under oxic conditions, microorganisms can carry out "luxury" uptake of phosphate and store phosphorus as intracellular polyphosphates. Under hypoxic or anoxic conditions, the polyphosphate pool is hydrolyzed, releasing phosphate back to the porewater. The role of vacuolated nitrate-storing sulfide oxidizing bacteria, such as *Thiomargarita* and *Beggiatoa*, in benthic phosphorus cycling is even more striking (Schulz and Schulz, 2005; Brock and Schulz-Vogt, 2011; Goldhammer et al., 2010). These microorganisms perform dissimilatory nitrate reduction to ammonium (DNRA) but also appear to uptake and release phosphorus. Working with *Thiomargarita*, Schulz and Schulz (2005) showed that subsurface TPO_4 peaks of $>200\,\mu M$ could be sustained by exceptional bacterial TPO_4 release rates of 500–1700 $nmol\,cm^3\,d^{-1}$. Moreover, Goldhammer et al. (2010) not only provided direct evidence for uptake and internal storage of TPO_4 by *Thiomargarita* and *Beggiatoa*, but they also showed that these bacteria mediate authigenic apatite precipitation under anoxic conditions. On the other hand, the phylogenetically and metabolically related bacteria *Thioploca* that inhabits the seasonally anoxic sediments off the Chilean coast appears not to perform luxury P uptake and release, or at least not at the time of sampling (Holmkvist et al., 2010).

In this paper we present a suite of biogeochemical data, including measured rates of bioirrigation, collected over a year at roughly monthly intervals at the Boknis Eck

Benthic fluxes in seasonally-hypoxic sediments

A. W. Dale et al.

Back | Close

Full Screen / Esc

Printer-friendly Version

Interactive Discussion

time-series station located at the entrance of the seasonally-hypoxic Eckernförde Bay (Germany) in the SW Baltic Sea. The highly transient features of the data are analyzed using a previous steady-state model that has been modified to account for the temporal changes in bottom water chemistry, organic matter fluxes and sediment mixing rates by animals (Dale et al., 2011). The principle motive for the modeling work is to interpret the major features of the data and quantify the fluxes of dissolved constituent fluxes to and from the sediment. We provide circumstantial evidence for TPO_4 release by *Beggiatoa* at rates that are in good agreement with the few literature data available. The abundance and distribution of these bacteria in the sediments has been documented previously by Preisler et al. (2007), and the cycling of nitrogen by *Beggiatoa* at Boknis Eck was investigated by Dale et al. (2011).

The present work exemplifies how the combination of time-series data and modeling can be a very powerful tool for accurately quantifying benthic solute exchange fluxes and identifying the response times of biogeochemical processes to O_2 depletion.

2 Material and methods

2.1 Study site

Boknis Eck is a narrow channel located at the northern entrance of Eckernförde Bay (54° 31′ N, 10° 20′ E) and has a maximum water depth of about 28 m. The deep waters are frequently ventilated in winter due to saline inflows from the Great Belt (Hansen et al., 1999). From mid March until mid September, vertical mixing is restricted by density stratification of the water column, which leads to pronounced periods of hypoxia during late summer due to microbial respiration of organic material in the bottom waters and sediment (Graf et al., 1983; Meyer-Reil, 1983; Hansen et al., 1999). Phytoplankton blooms dominated by diatoms and dinoflagellates generally occur in spring (March to April) and autumn (September to November). This causes an increase in benthic activity (Graf et al., 1983) and elevated fluxes of phosphate and ammonium (Balzer et al.,

1983). Autumn storms and a decrease in surface water temperature cause a mixing of the water column and ventilation of the deeper water layers with increased nutrient concentrations (Hansen et al., 1999). The oxygen penetration depth into the sediments is limited to the upper millimeters when bottom waters are oxic (Preisler et al., 2007) yet may be as high as 10 mm on occasions in the shallower sandier sediments at 18 m depth (Graf et al., 1983).

The sediments at the present study site (28 m water depth) are classified as fine-grained muds (<40 µm) with a carbon content of 3 to 5 wt% (Balzer et al., 1986). Calcium carbonate content is <2 % (Balzer et al., 1983; Orsi et al., 1996). With no significant terrestrial runoff, the bulk of organic matter within Eckernförde Bay sediments originates from marine plankton and macroalgal sources (Balzer et al., 1987; Orsi et al., 1996). Degradation and fermentation of organic matter produces free methane gas at Boknis Eck but fluid seepage from groundwater discharge has not been observed (Schlüter et al., 2000). The dominant fauna in the sediments in winter/spring are the polychaetes *Pectinaria koreni* and *Nephtys ciliate* with recorded abundances of 201–476 and 63–122 individuals m^{-2}, respectively (Graf et al., 1982). Specimens up to 10–15 cm long were present during winter in the cores retrieved in this paper. Mats of *Beggiatoa* were absent on the surface of Boknis Eck sediments during the period with oxygenated bottom waters, but are present below the sediment surface at the redox interface at the top of the sulfide layer (Preisler et al., 2007). In late summer 2010 when the bottom waters become almost anoxic, we observed a blackening of the surface sediments and colonization by *Beggiatoa* filaments.

2.2 Sampling and analytical methods

Sediment samples were obtained on 12 occasions between February and December 2010, which covers the major events of the year, that is, spring and autumn blooms, stagnation and severe hypoxia in late summer and winter dormancy (Graf et al., 1983). The sampling dates as well as temperature, salinity and dissolved oxygen (O_2) concentrations in the bottom water (25–28 m) measured using a CTD (Hydro-Bios, Kiel,

Title Page

Abstract | Introduction

Conclusions | References

Tables | Figures

◄ | ►

◄ | ►

Back | Close

Full Screen / Esc

Printer-friendly Version

Interactive Discussion

Germany) are shown in Table 1. The sediment sampling device was a mini multiple corer (MUC) equipped with 4 core liners (60 cm long) which retrieved sediment cores with a diameter of 10 cm and a maximal length of ca. 35 cm. In general, 2 cores were sampled on each occasion for geochemical analysis, although 2 additional cores were retrieved on 28 April using a benthic lander (Sommer et al., 2008). Upon return to the GEOMAR laboratory 2–3 h later, the cores were immediately transferred to a cool room (4 °C). Porewater from one core was sub-sampled anaerobically using rhizons® and from the other(s) by sectioning into 1–2 cm thick slices under ambient air and squeezing the sediment with low pressure argon (1 to 5 bar) through 0.2 µm cellulose acetate nucleopore® filters. Prior to use, the rhizons were preconditioned in an oxygen-free water bath. To ensure that the samples had not been in contact with air, the first 0.5 cm^3 of extracted porewater was discarded. All filtrates were collected in acid-cleaned recipient vessels and further manipulated for analytical determinations. Wet sediment samples (∼5 ml) were freeze dried for the determination of porosity from the water content using a dry sediment density of 2.5 g cm^{-3}.

The squeezed porewater samples were analyzed for the following solutes: sulfate (SO_4^{2-}), nitrate (NO_3^-), nitrite (NO_2^-), ammonium (NH_4^+), total hydrogen sulfide ($TH_2S \approx H_2S + HS^-$), ferrous iron ($Fe^{2+}$), total phosphate ($TPO_4 \approx H_2PO_4^- + HPO_4^{2-}$), bromide ($Br^-$), dissolved inorganic carbon ($TCO_2 = HCO_3^- + CO_3^{2-} + CO_2$) and total alkalinity (TA). The porewater sampled using rhizons was simultaneously analyzed for NH_4^+, Fe^{2+}, TPO_4 and TA. Analytical details for SO_4^{2-}, NO_3^-, NO_2^-, NH_4^+, TH_2S, TCO_2 and TA are described in Dale et al. (2011). Br^- was determined in the squeezed porewater by ion chromatography using a Metrohm ion chromatograph with a conventional anion exchange column with IAPSO seawater standard for calibration (relative precision of <2 % for natural seawater samples). For Fe^{2+} determination, 10 µl of concentrated HNO_3 was added to 1 ml of porewater and analyzed by ICP-AES with a precision of <2 %. All dissolved iron in the pore water was assumed to be present as Fe^{2+}. Dissolved phosphate was determined using photometry with a precision of 5 %. Systematic differences in the measured concentrations of the samples obtained by rhizons

and squeezed sediments could not be discerned. Therefore, although the data are presented according to the extraction method, they are not discussed individually.

In this paper, we also present rates of benthic sulfate reduction (SR) measured in parallel cores from April to December presented by Bertics et al. (2012). SR data from 5 and 6 March 2002 measured at the same location and published by Treude et al. (2005) are used to help interpret the data from 22 March 2010 in this study. Analytical details are presented by these authors.

2.3 Bioirrigation experiments

Throughout the duration of the sampling campaign, additional multi-cores (1 cm internal diameter) were taken to the home laboratory for manipulation experiments to determine bioirrigation rates. The procedure involves adding a large excess of a dissolved conservative tracer, in this case Br^-, to the water overlying the sediment and allowing the core to incubate for a known period of time. Posterior analytical determination of the depth distribution of Br^- allows the rate of irrigation to be approximated by modeling the transient infiltration of Br^- into the sediment using a numerical model (Martin and Banta, 1992).

Following delivery to the laboratory, the sediment cores were allowed to settle for a period of 24–48 h at 4 °C whilst stirring (60 rpm) the overlying water at approximately 20 cm above the sediment surface. Observed trajectories of small amounts of suspended particulate material at the bottom of the overlying water showed that this rate of stirring was sufficient to ventilate the surface of the sediment. It was not possible to control the dissolved O_2 concentration of the overlying water, and the cores were left open to air except during September and October when bottom water O_2 concentration was <5 µM. In these cases, the cores were bubbled with argon for 2 h and sealed tightly with the stirrer mounted through a rubber stopper. After the settling period, an excess of NaBr dissolved in a small amount of seawater was then added to the cores, so that the final Br^- concentration was ca. 20 mM. The cores were then allowed to incubate for 7 d (10 d on 22 March) in the dark with stirring without a lid (closed lid for the September

Title Page

Abstract | Introduction

Conclusions | References

Tables | Figures

◄ | ►

◄ | ►

Back | Close

Full Screen / Esc

Printer-friendly Version

Interactive Discussion

Discussion Paper | Discussion Paper | Discussion Paper | Discussion Paper | Discussion Paper

and October cores), after which the sediment cores were sectioned and sampled for analysis of Br⁻ and porosity following the same procedures outlined above. The incubation time was chosen based on results by Meile et al. (2005), who showed that the apparent rate of irrigation determined using excess Br⁻ changes rapidly during the first few days of incubation, and only reaches quasi- steady state after approximately 1 week when transient concentration gradients and fluxes associated with burrows are reduced (Boudreau and Marinelli, 1994). The presence of macrofauna in sieved (mm) sediment was noted but not measured quantitatively.

The measured Br⁻ concentration profiles were simulated using a non-steady state model which accounts for solute transport into the sediments by molecular diffusion and bioirrigation using a non-local source sink function (Boudreau, 1984; Emerson et al., 1984). Assuming that porosity does not change during the incubation period, the 1-D the mass conservation equation which describes the change in Br⁻ concentration (M) in the sediment with time is expressed as:

$$\varphi \frac{\partial \text{Br}^-}{\partial t} = \frac{\partial}{\partial z}\left(\varphi D \frac{\partial \text{Br}^-}{\partial z}\right) + \alpha_{\text{bi}}\varphi\left(\text{Br}_{\text{olw}} - \text{Br}^-\right) \tag{1}$$

where z (cm) is depth in the sediment, t (d) is time, α_{bi} (d^{-1}) is the depth-dependent bioirrigation coefficient describing solute pumping through animal burrows and Br_{olw} (M) is the time-dependent Br⁻ concentration in the well mixed overlying water. The sediment porosity, φ, was defined by fitting the exponential function $\varphi = \varphi(L) + (\varphi(0) - \varphi(L))e^{-z/z_{\text{por}}}$ to the measured data on each date where the parameters $\varphi(0)$ and $\varphi(L)$ are the porosity at the sediment-water interface and in compacted sediments, respectively, and z_{por} (cm) is the porosity attenuation length. $\varphi(0)$, $\varphi(L)$, and z_{por} were determined by least squares fits to measured porosity profiles. The in situ molecular diffusion coefficient, D (cm^2 d^{-1}), was calculated from the value in seawater ($D_W = 1\,\text{cm}^2\,\text{d}^{-1}$) at the incubation temperature (4 °C) and salinity of 20 using $D = D_W(1 - \ln\varphi^2)^{-1}$ (Boudreau, 1997).

The lower boundary condition was defined as a zero gradient ($\partial \mathrm{Br}^-/\partial z = 0$). The Br^- concentration at the sediment surface was calculated dynamically considering a diffusive boundary layer of thickness z_{diff}:

$$\varphi D \left.\frac{\partial \mathrm{Br}^-}{\partial z}\right|_{z=0} = D_W \frac{\mathrm{Br}_{\mathrm{olw}} - \mathrm{Br}^-(0)}{z_{\mathrm{diff}}} \qquad (2)$$

5 where $\mathrm{Br}^-(0)$ (M) is the Br^- concentration in the surface sediment layer directly below the diffusive sublayer (Boudreau, 1996). A value of 0.04 cm was chosen for z_{diff} (Forster et al., 1999).

Transport of Br^- into the sediments results in a decrease in Br^- concentration in the overlying water column. This is accounted for by dynamically modeling $\mathrm{Br}_{\mathrm{olw}}$ at each
10 time step by integrating the tracer concentration over the entire depth of the sediment (z_{max}):

$$\mathrm{Br}_{\mathrm{olw}} = \mathrm{Br}_{\mathrm{olw}}(t=0) - \frac{1}{h} \int_0^{z_{\mathrm{max}}} \varphi \mathrm{Br}^- \mathrm{d}z \qquad (3)$$

where h is the height of the overlying water column (ca. 20 to 30 cm). $\mathrm{Br}_{\mathrm{olw}}$ also serves as the upper boundary condition for Br^-, from which $\mathrm{Br}^-(0)$ is calculated at each time
15 step.

The depth-dependence of α_{bi} was described using the function:

$$\alpha_{\mathrm{bi}} = \alpha_{\mathrm{bi1}} \frac{\exp(\alpha_{\mathrm{bi2}} - z)}{1 + \exp(\alpha_{\mathrm{bi2}} - z)} \qquad (4)$$

where α_{bi1} (d^{-1}) is approximately equal to the rate of bioirrigation at the sediment surface and α_{bi2} (cm) controls the irrigation depth. This type of formulation allows for
20 a constant rate of irrigation in the sediment down to a depth equal to ca. α_{bi2} (Dale

et al., 2011) and better describes the data from Boknis Eck compared to the more commonly employed single exponential function (e.g. Martin and Banta, 1992).

To solve the model, the continuous spatial derivatives in Eq. (1) were replaced with finite differences (Boudreau, 1997). The resulting set of ODEs was solved using the NDSolve algorithm in MATHEMATICA 7.0 using the method of lines over 100 discrete depth intervals with a grid spacing increasing from sub-mm scale at the top of the model domain to sub-cm scale at the bottom (30 cm). The initial Br^- concentration in the sediment was assumed to be constant and set to the value measured in sediments below 20 cm in the parallel cores sectioned for geochemical analysis. This approach disregards the obvious concentration gradients in background Br^- in the upper 10 cm due to irrigation and seasonal salinity changes (see Sect. 3). Yet, since the Br^- tracer concentration in the overlying water was ca. 50 times greater than the ambient background concentration (0.4 mM), failure to account for these seasonal trends of Br^- in the initial condition creates a negligible error in the results. The model solutions were >99 % mass conservative.

The bioirrigation constants α_{bi1} and α_{bi2} were quantified by running the model transiently for the length of the incubation period and tuning their values until a good fit with the measured Br^- concentrations was obtained. To make this approach as objective as possible, a simple optimization routine was used. This consisted of running the model 10 000 times using random values of α_{bi1} and α_{bi2} chosen with the RandomReal function in MATHEMATICA. After each simulation, the root mean squared error (RMSE) of the modeled results versus the observations was calculated. The final parameter values were those giving the lowest RMSE (typically less than 1 mM).

Quantifying bioirrigation rates using this approach relies on several underlying assumptions, such as (i) addition of NaBr does not affect sediment respiration or irrigation rates, (ii) accumulation of Br^- released during POM mineralization is negligible compared to the addition of the tracer, (iii) transfer of the cores from local in situ temperature to the constant cool room temperature of 4 °C does not significantly affect bioirrigation, (iv) cumulative error due to uncertainty in porosity, water height and diffusive boundary

layer thickness is small (<10 %), and (v) no artifacts arise due to changes in dissolved O_2 concentration over the course of the experiment. With the exception of the latter, which is the most tenuous in our case, these assumptions have been substantiated on numerous occasions (Martin and Banta, 1992; Forster et al., 1999, 2003; Rao and Janhke, 2004; Sayles and Martin, 1995).

2.4 Development of a dynamic biogeochemical model

2.4.1 Transport processes and biogeochemical reactions

A steady state 1-D numerical reaction-transport model described previously (Dale et al., 2011) was applied transiently to quantify the sediment-water solute exchange rates over the year and test additional hypotheses with regard to phosphorus cycling. The model explicitly considers the transport and reaction of 11 solutes and 7 solids within the upper 40 cm of sediment. The model also includes nitrate stored within *Beggiatoa* vacuoles ($NO_{3\,bac}^-$) and in the Discussion the model is modified to include an intracellular P pool. Solutes include O_2, SO_4^{2-}, NO_3^-, NO_2^-, NH_4^+, TH_2S, TCO_2, Fe^{2+}, TPO_4, Br^- and methane (CH_4). TA was not modeled explicitly but calculated from the TH_2S the TCO_2 profiles and a mean measured porewater pH of 7.7 (not shown). Solid components consist of particulate iron oxyhydroxides ($Fe(OH)_3$) with an associated fraction of iron-bound phosphorus (Fe–P), particulate sulfide as pyrite (FeS_2) and particulate organic matter (POM). Previously, 3 POM pools, "Gi", of differing reactivity, i ($i = 1, 2, 3$, with reactivity $1 > 2 > 3$) were considered. Here, a fourth POM pool (G0) is included to account for fresh material deposited during the spring and autumn blooms.

Geochemical species are transported through the sediment by advective and diffusive processes. Bioirrigation is also considered for solutes and transport of $NO_{3\,bac}^-$ into the sediment is described analogously to bioirrigation (Dale et al., 2011). In this study, we also consider an additional non-local solute exchange due to rising gas bubbles upon which we elaborate further below. Using the traditional mathematical

approach (Berner, 1980; Boudreau, 1997), the concentration of aqueous species, C_a (mmol cm^{-3}), solid species, C_s (dry wt %) and intracellular nitrate, (C_b (mmol cm^{-3}), in 1-D along the vertical z-axis with time, t, can be described as:

$$\varphi \frac{\partial C_a}{\partial t} = \frac{\partial}{\partial z}\left(\varphi D \frac{\partial C_a}{\partial z} - \varphi v_a C_a\right) + \alpha_{bi}\gamma_{bi}\varphi(C_a(0) - C_a) \tag{5a}$$
$$+ \alpha_{bu}\gamma_{bi}\varphi(C_a(0) - C_a) + \varphi\Sigma R$$

$$(1 - \varphi)\frac{\partial C_s}{\partial t} = \frac{\partial}{\partial z}\left((1 - \varphi)D_b \frac{\partial C_s}{\partial z} - (1 - \varphi)v_s C_s\right) + (1 - \varphi)\Sigma R \tag{5b}$$

$$\varphi \frac{\partial C_b}{\partial t} = \alpha_b \varphi(C_b(0) - C_b) + \varphi R_{DNRA} \tag{5c}$$

where φ is steady state porosity, v_a (cm d^{-1}) and v_s (cm d^{-1}) are the burial velocities of porewater and solids, respectively, D (cm^2 d^{-1}) is the tortuosity corrected molecular diffusion coefficient, D_b (cm^2 d^{-1}) is the bioturbation coefficient, α_{bi} (d^{-1}) is the solute bioirrigation coefficient determined from the Br$^-$ incubations, $C_a(0)$ is the solute concentration at the sediment-water interface, α_b (d^{-1}) is the coefficient for non-local transport of nitrate by filamentous sulfide oxidizing bacteria, $C_b(0,t)$ is the intracellular nitrate concentration at the sediment-water interface, α_{bu} (d^{-1}) is the non-local exchange coefficient due to irrigation by rising methane gas bubbles and γ_{bi} is a dimensionless factor that scales the irrigation coefficients of the different solutes to that of Br$^-$. ΣR is the sum of the rate of change of concentration due to biogeochemical reactions and R_{DNRA} is the rate of DNRA. A detailed description of the model, including the relevant constitutive equations for the transport terms, is provided in the Supplement.

The biogeochemical reaction network is shown in Table 2. Most of these reactions have been discussed by Dale et al. (2011). Those which are newly described here relate to iron and phosphorus cycling (Fig. 1). Model parameters are given in Table 3. POM is a composite of organic C, N and P fractions defined as $CN_{(N:C)i}P_{(P:C)i}$, where

$(N:C)_i$ and $(P:C)_i$ are the ratios of organic N and organic P to particulate organic carbon (POC) in pool Gi. $(N:C)_i$ is specific to the Gi pool (see Supplement), whereas a constant $(P:C)_i$ value of 1/106 determined from in situ flux experiments was prescribed for all POM fractions (Balzer et al., 1983). POM is degraded by aerobic respiration, denitrification, dissimilatory iron reduction (DIR), sulfate reduction (SR) and methanogenesis, releasing TCO_2, NH_4^+ and TPO_4 to the porewater. The rate of POM mineralization at each depth is determined by the concentration of available electron acceptors using Michaelis-Menten kinetic limitation terms (Table 2). A nominal oxidation state of zero for POC is assumed.

Concentration profiles of Fe^{2+} and $Fe(OH)_3$ indicate that reduction of $Fe(OH)_3$ is an important component of the iron cycle in Boknis Eck sediments (Preisler et al., 2007). Therefore, and in line with previous studies (Berg et al., 2003; Dale et al., 2009a), $Fe(OH)_3$ was partitioned into a fraction termed $(Fe(OH)_{3-A})$ that is reduced during DIR and by reaction with dissolved sulfide and a fraction that reacts with sulfide only $(Fe(OH)_{3-B})$. The iron cycle also includes precipitation of iron sulfides (assumed to be FeS_2) and the oxidation of FeS_2 and Fe^{2+} by O_2. Bimolecular rate expressions that are first-order in reactants are prescribed for these reactions, with the exception of reductive dissolution of iron oxyhydroxides by dissolved sulfide which is half-order in sulfide (Poulton, 2003). Reported rate constant values for these reactions span many orders-of-magnitude and the values used here are based on other modeling studies where iron cycling is well-documented (Dale et al., 2012).

Fe–P is co-deposited to the sediment with iron oxyhydroxides (Fig. 1). The $P:Fe$ molar ratio in this particulate material (ε) is taken to be 0.1. Slomp et al. (1996) argued that this was a typical ratio for natural and synthetic poorly crystalline iron oxides (see references therein) and obtained good modeling results using this value. Dissolution of iron oxyhydroxides releases both Fe^{2+} and TPO_4 to the porewater. Authigenic iron oxyhydroxide precipitation (R_{Fe2ox}, Table 2) removes a fraction of dissolved TPO_4 and increases the Fe–P pool. However, this reaction mainly takes place in the thin oxidized sediment layer where the concentration ratio of Fe^{2+} to TPO_4 is often lower than ε.

Title Page

Abstract | Introduction

Conclusions | References

Tables | Figures

|◀ | ▶|

◀ | ▶

Back | Close

Full Screen / Esc

Printer-friendly Version

Interactive Discussion

Hence, uptake of TPO_4 into Fe–P cannot simply be equal to the rate of iron oxidation multiplied by ε because this would result in negative TPO_4 concentrations at the surface. To circumvent this problem, a phosphate-limiting term is included in the rate of TPO_4 removal associated with iron oxyhydroxide precipitation. The mass conserva-
5 tive rate of TPO_4 release during dissolution of iron oxyhydroxides is thus based on the relevant depth-dependent fraction of Fe–P to $Fe(OH)_3$ (θ in Table 2). Note that ε and $(P:C)_i$ are not treated as a fitting parameters initially, in order to highlight the potential shortcomings of the P cycle included in the model and to identify a possible source of TPO_4 from *Beggiatoa*.

10 ## 2.4.2   Time-dependent functions and boundary conditions

This section details the temporally-variable boundary conditions and functions used. Further details as well as information on the time-invariable boundary conditions are given in the Supplement.

   A major advance of this model compared to the previous steady state application
15 (Dale et al., 2011) is that the entire time series of porewater data and SR rates was used to constrain the biogeochemical reactions. The temporal variability in the data is driven by seasonal changes at the seafloor. To capture this dynamic, the model boundary conditions and forcing functions were varied intra-annually but not inter-annually until a new seasonally-cycling steady state was reached. This approach provides a unique
20 opportunity to more accurately parameterize several key transport and reaction terms compared to transient model applications constrained with data from a single sampling only.

   To start with, measured bottom temperatures were imposed in the model (Fig. 2a). Heat transfer is rapid through muddy sediment compared to molecular diffusion and
25 temperature changes at the sediment surface were assumed to immediately penetrate the modeled sediment column (40 cm) although this is only an approximation (Dale et al., 2008). Molecular diffusion coefficients and chemical reaction rates were corrected dynamically for temperature (Boudreau, 1997; Schulz, 2006), the latter by

Benthic fluxes in seasonally-hypoxic sediments

A. W. Dale et al.

Title Page

Abstract	Introduction
Conclusions	References
Tables	Figures

◀   ▶

◀   ▶

Back   Close

Full Screen / Esc

Printer-friendly Version

Interactive Discussion

multiplying the rate by an Arrhenius term, $f(T)$ (Table 2). The temperature response was broadly defined using a Q_{10} value of 3 for POM mineralization and 2 for secondary redox reactions. However, differential temperature responses for some reactions were included if supported by experimental evidence, for example denitrification and anammox. The change in bottom water salinity (21 ± 2.5; Table 1) was much less than for temperature (ca. $5 \pm 4\,°C$) and the effect of salinity on the diffusion coefficients was ignored. Salinity changes were nonetheless considered for major seawater ions (Br^-, SO_4^{2-}) whose upper boundary concentrations scaled to standard (IAPSO) seawater composition within a margin of 5 % (Fig. 2b). As an upper boundary condition for O_2, the measured bottom water concentrations based on the data in Table 1 and O_2 data gathered from the time series station during 2010 (Bange et al., 2011) were used (Fig. 2c). Although bottom water nutrient concentrations also fluctuate throughout the year in the bottom water (Dale et al., 2011), the trends are not obvious and ignored in the model. Thus, all bottom water solute concentrations except O_2, Br^- and SO_4^{2-} were fixed.

Fixed concentrations were defined at the lower boundary for SO_4^{2-}, TCO_2, NH_4^+, TH_2S, TPO_4 and CH_4 because their concentrations in the modeled domain are influenced by POM mineralization at greater depth (Dale et al., 2011). All other solutes at the lower boundary were defined with a zero concentration gradient (Neumann condition). Lower boundary conditions for all variables were time-invariable.

The upper boundary concentration for intracellular nitrate ($NO_{3\,bac}^-(0)$) was set to the porewater normalized concentration (150 µM) measured in sediment samples from Boknis Eck that were repeatedly frozen and thawed to release nitrate stored within *Beggiatoa* (Preisler et al., 2007). Previously, we set this boundary condition to bottom water nitrate concentrations (Dale et al., 2011). We have revised this approach for consistency with modeling studies at other sites where porewater normalized $NO_{3\,bac}^-$ concentrations were used (Dale et al., 2009a; Bohlen et al., 2011).

In the previous model (Dale et al., 2011), DNRA showed a maximum rate in the upper 5 cm as shown by Preisler et al. (2007), with an attenuated rate down to the

bioirrigated depth (10 cm). When the complete set of data was analyzed, however, we were able to refine this further by restricting the depth of intracellular nitrate transport to 5 cm. This better agrees with measured *Beggiatoa* biomass concentrations at different times of the year (Preisler et al., 2007). We observed *Beggiatoa* filaments at the sediment surface during hypoxia and very low sulfide concentrations in the upper 5 cm in October and November. Based on previous results in sediments with *Thioploca* (Holmkvist et al., 2010) it is likely that the higher biomass maintained these low sulfide concentrations. The rate of nitrate transport was therefore increased in October and November to simulate the sulfide profiles. The sulfide depletion lags behind the minimum in O_2 by around 1 month (see Sect. 3), which may reflect the time delay for the *Beggiatoa* biomass to respond to increasing hypoxia at the sediment surface. Thus, nitrate transport (Fig. 2d) was dependent on the time-lagged O_2 concentrations (O_2') shown in Fig. 2c.

The rate constant for reductive dissolution of iron oxide particles, k_{Fe3red}, was made to be dependent on oxygen O_2' (Table 2). An explanation is given in Sect. 4.

POM fluxes to the sea floor have been reported to be 0.4 to 0.59 mmol C cm^{-2} yr^{-1} based on in situ total oxygen uptake measurements in the deep channel at 28 m (Balzer et al., 1986). This flux is composed as a continuum of reactive fractions, parameterized in this study using a multi-G approach consisting of 4 POM pools. The total flux of the less reactive G2 and G3 pools has been quantified as 0.12 mmol C cm^{-2} yr^{-1} (Dale et al., 2011). Due to the recalcitrant nature of these fractions, seasonal changes in their flux will have a negligible effect on solute dynamics in the upper 40 cm. G2 and G3 fluxes are therefore time-invariable, which leaves up to 0.47 mmol C cm^{-2} yr^{-1} to be split between the reactive G0 and G1 fractions. G0 and G1 fluxes were time-dependent. The temporal variability in G1 flux was calculated by first integrating measured sulfate reduction rates over the upper 15 cm (Bertics et al., 2012). Multiplying these rates by 2 provides the carbon mineralization rate, assuming a carbon oxidation state of zero. Dividing these rates by $f(T)$ (Table 1) corrects for changes in temperature and provides an estimate of the G1 flux. Yet, these fluxes are minimum values since G1

is also oxidized by other electron acceptors such as O_2 and NO_3^-. Therefore, the flux of G1 was constrained with the model by increasing the flux proportionally over the year until a good fit was made with the measured SR rates. When integrated over the year, this amounted to $0.42\,\text{mmol}\,C\,cm^{-2}\,yr^{-1}$. This leaves $0.05\,\text{mmol}\,C\,cm^{-2}\,yr^{-1}$ for G0, which was split evenly over the spring (March–April) and autumn ($\sim$ September) blooms. Fluxes of G0 and G1 (in $\text{mmol}\,C\,m^{-2}\,d^{-1}$) used in the model are shown in Fig. 2e.

As a first approximation, the fluxes of particulate iron pools to the seafloor were time-invariable. FeS_2 was set to zero. The total flux of iron oxyhydroxides was estimated from mass accumulation rates and iron concentrations at a nearby site (Balzer, 1982; Lapp and Balzer, 1993). This flux was divided equally into $Fe(OH)_{3\text{-A}}$ and $Fe(OH)_{3\text{-B}}$.

Bioturbation is limited to the upper few cm in Boknis Eck (Dale et al., 2011). The seasonal variability is unknown, but the rate of mixing is likely diminished in autumn when hypoxia is established and macrofauna are absent. Thus, the biodiffusion constant, $D_b(0)$, was scaled to O_2 (Fig. 2f) so that in February $D_b(0)$ is equal to ca. $0.08\,\text{cm}^2\,d^{-1}$ (Dale et al., 2011).

Bioirrigation coefficients α_{bi1} and α_{bi2} derived from the tracer incubations were imposed directly in the model and are described in Sect. 3. The parameter γ_{bi} that defines solute specificity of the irrigation parameters is detailed in the Supplement. Note that because of rapid oxidation of Fe^{2+} and precipitation of authigenic iron oxyhydroxides on burrow walls, Fe^{2+} is not transported by bioirrigation (Meile et al., 2005).

The bubble irrigation coefficient, α_{bu}, was prescribed a constant value over a defined depth:

$$\alpha_{bu}(z) = \begin{cases} \alpha_{bu}(z), & \text{if } z < z_{bu} \\ 0, & \text{if } z \geq z_{bu} \end{cases} \tag{6}$$

where z_{bu} (30 cm) is the maximum depth where the porewater are strongly affected by bubble irrigation. Irrigation of sediment porewater by gas rising through open bubble

Benthic fluxes in seasonally-hypoxic sediments

A. W. Dale et al.

tubes or vacant animal burrows was proposed by Martens in 1976 and the theory developed further by Haeckel et al. (2007). These authors described how bubbles enhance diffusive mixing in their wake as they rise through tube structures and act as an abiotic irrigation process by homogenizing concentration gradients between the sediment and the overlying seawater. The idea of using constant rates of irrigation down to a specific depth is based on simulations of sediments affected by CH_4 gas venting in the Sea of Okhotsk (Haeckel et al., 2007). Although a mechanistic theory which explains this phenomenon has not been reported, the gas bubbles may manage to form their own small fractures and tubes in the muddy, unconsolidated near surface sediments (Algar et al., 2011). Once these high permeability conduits are formed, rising bubbles reach a terminal rise velocity and are released rapidly from the sediment to the water column (Haeckel et al., 2007). Bubble irrigation is defined analogously to bioirrigation using the same solute specific factors, γ_{bi} (Eq. 5a). The depth, intensity and duration of bubble irrigation events in Boknis Eck were estimated from the entire suite of data, but mainly from SO_4^{2-}, NH_4^+, TH_2S, TCO_2 and TA. The temporal change in α_{bu} is shown in Fig. 2h.

Following the gas irrigation events a rapid steepening of the SO_4^{2-}, H_2S, TCO_2 and TA gradients, indicative of enhanced sulfate reduction, was observed in the following months (see Sect. 3). We argue that the newly opened bubble conduits provide an avenue for a residual reservoir of smaller methane bubbles to travel slowly upward, dissolve and consume SO_4^{2-} by anaerobic oxidation of methane (AOM, R_{AOM} in Table 2) producing H_2S and TCO_2. We simulated the net effect of this process by imposing an upward advection term for CH_4 only (Fig. 2h). The rate of advection was constrained from the SO_4^{2-}, H_2S, TCO_2 and TA concentrations. A time lag of around 1 month for this process following bubble irrigation was found to provide the best correspondence with the data.

2.4.3 Model uncertainties and solution

Although the data in Fig. 2 are resolved at approximately monthly intervals, there are several caveats to consider assuming that these forcing functions are constant from year-to-year. Firstly, random fluctuations in the boundary conditions are very likely oc-
5 curring on shorter timescales. Secondly, the progressive decline in mean O_2 levels and increase in mean temperature since the 1950s is not accounted for (Bange et al., 2011). The effect of these changes is considered to be small compared to those arising from the intra-annual variations and to have no significant bearing on the results presented here. Thirdly, Arntz (1981) argued that the benthic community assemblage at any given
10 time is determined by the length and severity of hypoxia over the previous years. This influences the rate and depth of bioturbation, bioirrigation and the redox potential of the surface layers, potentially leading to a variable oxygen debt from year-to-year via the accumulation of reduced geochemical species (Graf et al., 1983).

In view of these uncertainties, it is not our intention to simulate every detail of the
15 measured geochemical data. This would require an excess of tunable parameters, lead to a lack of transparency and devalue the conclusions. Instead, by maintaining a realistic level of model complexity, our objective was to simulate the major transient features of the data and relate these to fluxes across the sediment-water interface. The model presented consists of a complex set of reactions and many adjustable parame-
20 terizations. In actuality, most of the parameters are constrained from field observations at Boknis Eck or from literature studies that demonstrate either experimentally or the-oretically the assignment of a value to a given parameter. The sensitivity of the model to the nitrogen cycling in the model has been dealt with previously (Dale et al., 2011) and in this work we detail the areas where more research effort is needed to more
25 accurately quantify iron and phosphorus cycling.

The model was solved in the same way as described above for bioirrigation and by Dale et al. (2011). A high resolution of 0.06 cm was used at the surface to minimize numerical errors and determine reliable gradients within these highly reactive layers.

Benthic fluxes in seasonally-hypoxic sediments

A. W. Dale et al.

Title Page

Abstract | Introduction

Conclusions | References

Tables | Figures

◀ | ▶

◀ | ▶

Back | Close

Full Screen / Esc

Printer-friendly Version

Interactive Discussion

At the base of the sediment the grid thickness increased to 0.7 cm. A centered finite difference scheme was used for dissolved species and solid species within the bioturbated zone. An upward scheme was applied for the transport of solids below this depth to avoid numerical instabilities (Boudreau, 1996). Adopting this approach, the model simulations were stable despite the often abrupt change in boundary conditions and forcings. The model was run in a seasonally-cycling transient model that required ca. 600 yr to reach a dynamic steady state. Mass conservation was checked by annually integrating daily fluxes, resulting in a mass balance generally $\gg 99\%$ for all species.

3 Results

Measured and modeled Br^- concentrations in the incubated cores indicate a general trend of high bioirrigation rates in winter with well-oxygenated bottom waters and low or zero bioirrigation during the hypoxic summer and autumn period (Fig. 3). In winter (23 February), Br^- concentrations in the upper 10 cm at the end of the incubation varied little from the bottom water concentration (16 mM), coincident with the greatest depth where polychaetes were observed, and then decreased steadily down to 20 cm. The corresponding modeled Br^- tracer profile using Eq. (1) provides a very close correspondence with the measured data with values of α_{bi1} and α_{bi2} of 0.28 d^{-1} and 12.8 cm, respectively, indicating near constant irrigation rates to almost 12 cm. This is very different from the theoretical profile considering transport of Br^- into the sediment by molecular diffusion only where Br^- diffuses down to ca. 8 cm. Deep irrigation did not re-occur over the sampling period. The same trends are mirrored in the concentrations of all solutes (with the exception of Fe^{2+}), which display near-constant concentrations in the upper 10 cm in February at values equal to those measured in the bottom water (Fig. 4).

Between February and April, α_{bi1} remained high yet then fell dramatically to 0.03 d^{-1} in July. The porewater concentration gradients in the upper 10 cm also became more pronounced over this period (again excluding Fe^{2+}). The measured Br^- tracer

Benthic fluxes in seasonally-hypoxic sediments

A. W. Dale et al.

concentration in July showed a similar distribution to the diffusion-only profile, coincident with a drop in bottom water O_2 to 70 μM (Table 1). This value is very close to the reported threshold for hypoxia (~63 μM O_2), at which large changes are engendered in community structure by oxygen stress (Diaz and Rosenburg, 2008). Although O_2 continued to fall in August (47 μM), α_{bi1} and α_{bi2} inexplicably increased again to 0.08 d^{-1} and 9.6 cm, respectively. Whilst it is possible that this could highlight increased pumping by the benthic community to compensate for low oxygen levels (Forster al., 2003), we are hesitant about these values since they could reflect artefacts caused by removal of the core under hypoxic bottom waters and incubation under atmospheric conditions.

From September, α_{bi1} fell to low levels of <0.01 d^{-1}, essentially indicating a complete absence of bioirrigation as bottom waters became almost anoxic (2 μM O_2). No polychaetes were observed in these cores due to mortality or migration to shallower waters and dead polychaetes were observed on the sediment surface. The Br$^-$ tracer concentration at this time was indistinguishable from the diffusion-only profiles, as observed on a previous visit to this site (Forster et al., 1999). Interestingly, the sediments became more compacted between August and October with porosity at 2 cm decreasing from an average of 0.91 in winter to 0.88 (Fig. 3). This 30 % increase in solid volume fraction $(1 - \varphi)$ is presumably a result of the partial collapse of relic burrows. Bioirrigation rates did not recover in November and December even though the bottom waters were again well-oxygenated due to mixing of the water column by autumnal storms (Table 1). No polychaetes were recovered from the sediments in November and December. This confirms previous observations that a time lag of at least 2 months is required following hypoxia before the sediments at Boknis Eck become habitable to macrofauna (Meyer-Reil, 1983).

Despite the lack of irrigation from September onwards, the concentration gradients of TCO_2, NH_4^+ and TA did not accumulate in response to temperature-induced increase in organic matter degradation as expected from time-series data elsewhere (e.g. Klump and Martens, 1989). On the contrary, TCO_2 concentrations decreased from 12 to 7 mM at 20 cm depth between September and October (Fig. 4a), NH_4^+ fell by a factor of 2

Title Page

Abstract | Introduction

Conclusions | References

Tables | Figures

◄ | ►

◄ | ►

Back | Close

Full Screen / Esc

Printer-friendly Version

Interactive Discussion

from 1500 µM to 700 µM (Fig. 4f), and TH$_2$S decreased by at least a factor of 4 (Fig. 4i). Conversely, SO$_4^{2-}$ concentrations at depth began to increase at this time (Fig. 4c). This rate of concentration change is much faster than can be explained by molecular diffusion and resembles deep irrigation. Shortly afterwards, extremely high SR rates were measured in two of the triplicate cores in November (Fig. 4e). This perturbation in solute concentrations was not, however, an isolated incident and similar trends were observed for NH$_4^+$, TPO$_4$ and SO$_4^{2-}$ in May.

Fe^{2+} and TPO$_4$ behaved quasi-independently of the other solutes (Fig. 4g, h). Fe^{2+} exhibited a peak approaching 194 µM on 23 February, which then diminished in March and disappeared completely by July. In contrast to Fe^{2+}, TPO$_4$ concentrations were maintained at low levels in the bioirrigated zone in winter. From August onwards, the Fe^{2+} peak slowly reappeared and extended downwards, reaching 180 µM at 1 cm depth in October and 311 µM at 3 cm depth in November. Furthermore, the entire Fe^{2+} peak extended over the upper 1 cm in November compared to 2 cm in October. Similarly, TPO$_4$ was elevated over the upper 6 cm and 10 cm in October and November, respectively, where extremely high concentrations in excess of 437 µM were measured. The increase in vertical extension of the Fe^{2+} and TPO$_4$ peaks between October and November coincides with a depletion of sulfide to levels below detection limit (Fig. 4i).

The modeled concentration and SR rate profiles are shown alongside the measured data in Fig. 4. Imposing the transient forcings and boundary conditions in Fig. 2, the model reproduces the major trends in the data to a high degree with the exception of the TPO$_4$ concentrations in the upper 10 cm during the hypoxic season. These include (1) the constant concentrations in the upper 10 cm in winter, (2) the shallowing of the concentration gradients in May and October/November, and (3) the iron peaks in winter and autumn. The first two of these observations are consistent with non-local solute exchange by bioirrigation and bubble irrigation, respectively.

4   Discussion

4.1   Benthic-pelagic solute exchange processes and rates

The near-constant concentrations of SO_4^{2-}, TA, TCO_2, NH_4^+, TPO_4 and TH_2S in the upper 10 cm in February at values equal to those measured in the bottom waters is strong evidence for non-local exchange of porewater with seawater by the pumping action of indwelling fauna. This process ameliorates the classic fingerprint of organic matter degradation in the surface sediment layers (Dale et al., 2011). Sediments only became sulfidic below 10 cm in the sulfate reduction zone, which corroborates previous measurements using microelectrodes (Preisler et al., 2007). Between February and April, the depth of irrigation decreased by more than a factor of 2 allowing TCO_2, NH_4^+, PO_4^{3-} and TH_2S to accumulate and SO_4^{2-} to become more extensively depleted. More intense bioirrigation at the start of winter may be explained by tube building activities of the pioneering polychaete population following the previous hypoxic season (Meyer-Reil, 1983).

Attributing the transient nature of these concentration profiles to bioirrigation rather than geochemical processes is consistent with the model results that closely simulate the data using the rates of bioirrigation derived from the Br^- incubations. The irrigation coefficient for February ($\alpha_{bi1} = 0.34\,d^{-1}$) is similar to the higher end irrigation coefficients of ca. $0.38\,d^{-1}$ reported for the Southern North Sea and Kiel Bight (Forster et al., 2003; Schlüter et al., 2000). The biogeochemical model also simulates the natural Br^- abundance in February (Fig. 4d). The data-model disagreement for Br^- at 10 cm depth is likely due to spatial differences in biomass abundances in the cores sampled for geochemistry and incubation experiments. In addition, NH_4^+ and NO_3^- fluxes measured ex situ during winter by Dale et al. (2011) were many-fold higher than the molecular diffusive fluxes. Enhanced diffusion of this type is often ascribed to bioirrigation (Glud et al., 1994).

When the modeled daily solute fluxes across the sediment-water interface are compared, it is clear that bioirrigation accounts for most of the transport to and from the sediment in winter at Boknis Eck (Fig. 5). Even though the relative importance of bioirrigation tails off as the year progresses, non-local exchange by gas bubbling clearly dominates transport for some species at discrete intervals beginning in May (e.g. TCO_2, NH_4^+ and TH_2S), with two further ebullition events in September and late October. The bubble irrigation rate constant determined from the solute concentration profiles is an order-of-magnitude lower than that for bioirrigation (Fig. 2h). Yet, because it extends over a much greater depth (~ 30 cm) where TCO_2, NH_4^+ and TH_2S accumulate at high concentrations, it has a profound effect on their fluxes across the sediment-water interface. The occurrence of TH_2S in the bottom waters during the anoxic period (Balzer et al., 1983; Ehrhardt and Wenck, 1984; Bange et al., 2010) could well be a result of bubble-associated release. Porewater-seawater exchange by rising bubbles has the potential to shift a large part of the oxygen demand, supplied initially as POM, from the sediment to the water column in the form of TH_2S and CH_4. How these fluxes will develop in the future and their potential to intensify or prolong hypoxia is a topic for future investigation.

Highly reactive species such as O_2 and NO_3^- are mainly consumed in the surface sediment layers, which creates a high flux through the diffusive boundary layer. Averaged over the year, 60 % of O_2 and NO_3^- enter the sediment by diffusion, compared to <10 % for bubble irrigation. Up to 75 % of POC is degraded aerobically in winter, which reflects the presence of reactive carbon within the surface oxidized layer (Fig. 6a). Overall, POC mineralization oscillates between aerobic respiration in winter and spring to sulfate reduction in summer and autumn, with other carbon degradation pathways playing a minor role.

A large spike in O_2 consumption of 26 mmol m^{-2} d^{-1} occurs prior to the spring bloom (Fig. 5b). Following the spring bloom, oxygen uptake is lower (15 mmol m^{-2} d^{-1}). Interestingly, total oxygen consumption from 1 January to the start of the spring bloom in March is 1100 mmol m^{-2}, compared to a POC deposition flux of only 800 mmol m^{-2}.

This difference represents the oxygen-debt carried over from the previous hypoxic season when organic matter, pyrite and other reduced substances accumulated. This debt is quickly burned off in the following winter when deepwater renewal and invasion of irrigating organisms once again ventilate the upper sediments. The modeled oxygen uptake rates at this time of year agree with benthic respiration rates of 16 to 24 mmol m^{-2} d^{-1} made at the same time using landers (Sommer et al., unpublished).

When O$_2$ levels are diminished during hypoxia, diffusive fluxes of nitrate become elevated (Fig. 5b). At this time, the most reactive POM fractions are consumed by denitrification, which reaches maximum levels of 0.24 mmol m^{-2} d^{-1} in September when bottom water O$_2$ is 2 µM (Fig. 6c). Denitrification consumes only a few percent of POC (Fig. 6a) compared to 10 % on the continental shelf (Middelburg et al., 1996). This is because bottom water NO$_3^-$ concentrations are only 5–6 µM at Boknis Eck compared to >30 µM on the shelf. Furthermore, the low O$_2$ concentrations limit the potential for coupled nitrification–denitrification.

Following the peak in denitrification, DNRA rates increase sharply to 0.5 mmol m^{-2} d^{-1} in November (Fig. 6c). This is far less than 3.0 mmol m^{-2} d^{-1} on the Peruvian OMZ and 16 mmol m^{-2} d^{-1} in the highly reactive sediments of the Namibian shelf inhabited by giant sulfide oxidizers (Bohlen et al., 2011; Dale et al., 2009a). Presumably, more extensive periods of anoxia in these environments permit a higher build-up of biomass, which could explain why higher nitrate transport coefficients of 0.7 and 1.1 d^{-1} were calculated for these environments (Bohlen et al., 2011; Dale et al., 2009a) compared to maximum values of 0.12 d^{-1} in Boknis Eck (Fig. 2d). The NH$_4^+$ produced by DNRA exits the sediment by diffusion, leading to maximum simulated diffusive fluxes at this time of year which agree well with the measured values (Fig. 5).

4.2 Evidence for solute exchange by bubble irrigation

The experiments and modeling show that bioirrigation can be ruled out as the principle cause for the unusual shallowing of the solute concentration gradients in

Benthic fluxes in seasonally-hypoxic sediments

A. W. Dale et al.

Title Page

Abstract | Introduction

Conclusions | References

Tables | Figures

|◄ | ►|

◄ | ►

Back | Close

Full Screen / Esc

Printer-friendly Version

Interactive Discussion

October/November and, by extension, in May. The alternative hypothesis concerning bubble irrigation obviously requires independent experimental verification, but adds to a growing body of evidence which suggests that this process could be widespread in gassy coastal sediments. Irrigation of sediment porewater by rising gas bubbles was identified and quantified in Cape Lookout Bight sediments several decades ago (Martens, 1976; Martens and Klump, 1980; Klump and Martens, 1981). These studies have highlighted bubble transport as the major source of pelagic CH_4 in shallow water columns during summer. More recently, meter-scale irrigation patterns of SO_4^{2-} in sediments overlying gas hydrates have been attributed to ascending gas bubbles (Haeckel et al., 2007; Schwalenberg et al., 2010). It is worth noting that hydrodynamically-induced flushing of relic burrows by bottom currents (Ray and Aller, 1985) can be ruled out for Boknis Eck since the rapid changes in solute concentrations extend much deeper than the bioirrigation depth (ca. 10 cm).

There are several lines of evidence in support of CH_4 gas escape at Boknis Eck. To begin with, free gas is a common occurrence in the sediments throughout Eckernförde Bay, including Boknis Eck (Abegg and Anderson, 1997; Orsi et al., 1996), and bubble release has been observed in some parts of the bay (Jackson et al., 1998). Free gas occurs when the dissolved concentration exceeds the in situ solubility, and the depth at which gas forms depends on the mud thickness and the amount and reactivity of organic carbon contained within it (Dale et al., 2009b; Jensen and Bennike, 2009). Model simulations suggest that CH_4 saturation is reached at ca. m below the seafloor at Boknis Eck (Dale et al., 2011), although some degree of seasonal variability in this depth is to be expected (Wever and Fiedler, 1995; Mogollón et al., 2011).

In agreement with these studies, Bange et al. (2010) reported episodic CH_4 concentrations in excess of 230 nM in the bottom waters of Boknis Eck (25 m) during 2006–2008. Interestingly, when aggregating the data, a pattern emerged of highest CH_4 concentrations in early autumn (September–October) with another, albeit less obvious, concentration spike in late spring (March–April). This dovetails with the porewater data that also shows evidence for strong bubble release during the same periods, and may

further suggest that CH_4 release is triggered by a periodic forcing. Bange et al. (2010) postulated that the deposition of the spring and autumn blooms is responsible for releasing CH_4. The porewater data instead suggest that the CH_4 originates from the gas-bearing layers located well below the surface sediment layers where fresh phytodetritus is degraded. The autumn CH_4 release is more likely to be instigated by the high bottom water temperature, which rose to maximum values of $10\,°C$ at this time of year (Table 1). If the mean annual temperature is $5\,°C$, then a $5\,°C$ temperature increase in October would decrease CH_4 solubility by roughly $1\,mM$ (Duan et al., 1992). Using the equations given in Martens et al. (1998) and a porosity of 0.8, the evolved CH_4 gas would increase the volume of free gas by ca. $0.5\,\%$ for the ambient conditions of Boknis Eck. This is around one third of the peak gas volume of $1.5\,\%$ predicted for this site (Dale et al., 2011). Such an increase could lead to gas overpressure, degassing and non-local mixing of porewater with bottom water. In May the temperature was relatively low ($3.8\,°C$, Table 1) and we postulate that excess CH_4 gas that has accumulated over the winter may be released in spring as a sediment "burp" as temperatures start to rise. Changes in hydrostatic pressure due short-term sea level variations are also known to trigger CH_4 release from the sea floor (Martens and Klump, 1980).

Following the irrigation event in October, the SR rates in two of the triplicate subcores in November were extremely elevated below $20\,cm$ (Bertics et al., 2012), being up to 10 times higher than those measured at the same depth in previous months (Fig. 4e). We speculate that a fraction of this SR is associated with anaerobic oxidation of methane (AOM, R_{AOM} in Table 2). A large discharge of gas through sediment conduits in October could have opened a pathway for smaller pockets of CH_4 gas to advect slowly upwards as the system relaxed following the initial eruption. Lateral dissolution of gas through the walls of cracks and fissures would be assisted by CH_4 consumption by AOM which causes the porewater to become undersaturated with CH_4 (Mogollón et al., 2011). Further recent evidence from methane vents suggests that methanotrophic microbial biofilms could exist directly on the walls of sediment bubble tubes (Briggs et al., 2011). Potential AOM rates of $100\,nmol\,cm^3\,d^{-1}$ have been

measured at this site (Treude et al., 2005, indicating that CH_4 is not the only electron donor for SR. A pocket of extremely labile organic material may have been sampled, possibly consisting of dead polychaetes (Bertics et al., 2012). Despite these uncertainties, it is important to note that the steepening of the SO_4^{2-}, TA and TCO_2 gradients between November and December occurs far too quickly to be explained by molecular diffusion. This alludes to a modification of solute concentrations by a rapid increase in microbial activity.

4.3 Iron and phosphorus remobilization and fluxes

The transient Fe^{2+} peaks in winter and autumn represent a decoupling between Fe^{2+} source-sink processes (Fig. 4h). The winter maximum was predicted to be driven by re-oxidation of iron sulfides. Renewed deep ventilation of the sediments in winter by faunal activity exposes to oxidation reduced iron that had accumulated during the previous hypoxic season (Fig. 6b). Given that O_2 penetration into the sediment is <1 cm in winter (Dale et al., 2011), deep ventilation by bioirrigation drives most of the pyrite oxidation in the upper 10 cm. Because pyrite oxidation is not associated with TPO_4 release, TPO_4 and Fe^{2+} concentrations below the oxidized layer were decoupled in winter and no TPO_4 peak was observed (Fig. 4g).

An additional source of Fe^{2+} that was not considered in the model is from siderite ($FeCO_3$). Siderite can be associated with pyrite in fully marine and brackish sediments, possibly because of micro-environments that allow both minerals to be thermodynamically stable (Haese et al., 1997; Postma, 1982). The decrease in alkalinity during winter could have induced siderite to dissolve. The quantitative significance of siderite in surface marine sediments is generally believed to be minor, however, since its formation is inhibited by low levels of sulfide and siderite tends to be maintained below saturation due to proton release from POC mineralization processes (Haese, 2006; Jourabchi et al., 2005).

Despite this source of Fe^{2+}, the diffusive fluxes calculated from the porewater gradients at the sediment surface remain relatively low in winter at $0.2 \pm 0.05\,mmol\,m^{-2}\,d^{-1}$ (Fig. 5). Fe^{2+} that is released or diffuses into the surface oxidized layer is rapidly reoxidized to iron oxyhydroxides (Pakhomova et al., 2007; Severmann et al., 2010). Sequestration of TPO_4 onto freshly precipitated iron oxyhydroxides is a major control on TPO_4 fluxes in environments with high bottom water O_2 concentrations (Froelich et al., 1979, 1988; Krom and Berner, 1981; McManus et al., 1997). This authigenic P sink explains the low diffusive TPO_4 fluxes in winter (Fig. 5) and leads to extremely high C/P diffusive flux ratios of 710 for the diffusive fluxes across the sediment-water interface (Fig. 7). The C/P ratio still remains above Redfield at 113 in March. Despite this efficient trapping of TPO_4, the intense bioirrigation occurring at Boknis Eck in winter creates a bypass for TPO_4 to enter the water column with maximum predicted rates of $0.5\,mmol\,m^{-2}\,d^{-1}$ (Fig. 5). This is likely a maximum value due to the potential adsorption of TPO_4 onto iron hydroxides lining animal burrow walls (see below).

In autumn, when the surface oxidized layer was almost absent, diffusive Fe^{2+} fluxes increased by a factor of 4 from winter to $0.8 \pm 0.4\,mmol\,m^{-2}\,d^{-1}$ (Fig. 5). The TPO_4 diffusive fluxes calculated from the porewater gradients in October and November were $0.7 \pm 0.2\,mmol\,m^{-2}\,d^{-1}$ and $0.6 \pm 0.1\,mmol\,m^{-2}\,d^{-1}$, respectively (Fig. 5). These are identical to those reported by Balzer et al. (1983) for low O_2 conditions ($<1\,\mu M$) using a benthic chamber deployed at the same site. Enhanced P release leads to low C/P regeneration ratios of ca. 9 in September (Fig. 7), indicating extreme P enrichment of the fluxes relative to TCO_2. A TPO_4 flux of $0.7\,mmol\,m^{-2}\,d^{-1}$ over the 40 day hypoxic period (Fig. 6) would raise TPO_4 concentrations in the overlying water column (28 m) by around $1\,\mu M$. A potential further increase in TPO_4 flux is provided by the bubble release pathway. Excess benthic P regeneration forces the pelagic N/P ratio of dissolved inorganic nutrients in the water column below 6 (Smetacek et al., 1987), and may affect local productivity patterns as studies in other shallow ecosystems indicate (Rozan et al., 2002). The feedbacks on primary production and the timing of the autumn bloom

in Boknis Eck by benthic P release are suspected to be important but have not been investigated quantitatively (Smetacek et al., 1987).

As in winter, the presence of a peak in free Fe^{2+} during hypoxia suggests that the rate of pyrite formation is slow relative to reductive iron dissolution (Fig. 4h). We were only able to simulate the autumn Fe^{2+} peak by scaling the rate for reductive dissolution of iron oxyhydroxides to the time-lagged O_2 concentration (Fig. 2c, Table 2), effectively decoupling this reaction from FeS_2 precipitation. Otherwise, FeS_2 precipitation keeps pace with reductive dissolution of iron oxyhydroxides and maintains Fe^{2+} at low concentrations (data not shown).

This dependence of iron reduction on O_2 could reflect a missing or poorly represented process in the model. Although the time-lagged O_2 concentration appears to be related to enhanced nitrate transport by *Beggiatoa*, we are hesitant about linking these two aspects without further supporting data. The apparent dependence of iron oxyhydroxide dissolution on O_2 may be an artifact reflecting the simple 1-D bioirrigation function that fails to account for geochemical gradients around burrow walls (Meile et al., 2005; Meysman et al., 2006). Inhabited burrows are ventilated by the pumping action of the host organism, leading to a thin veneer of iron oxyhydroxides on the exposed burrow walls (Meile et al., 2005). Dissolution of iron oxyhydroxides following vacation of the burrows in response to hypoxia could increase Fe^{2+} concentrations in the burrow water, leading to the situation where horizontal chemical gradients exceed those in the vertical (Lewandoski et al., 2007; Meile et al., 2005). This heterogeneity is destroyed when porewater for geochemical analysis is extracted by squeezing the sediment or by using rhizons inserted laterally through the core. A test of the potential importance of iron cycling within animal burrows requires a higher dimensional model that explicitly considers tube geometry (Meile et al., 2005).

At this stage, only a causal relationship between the rate of iron reduction and O_2 concentrations can be established. Nevertheless, the important point is that the simulated Fe^{2+} peak in November represents the net uptake of Fe^{2+} into sulfidic minerals and Fe^{2+} release from dissolution of iron oxyhydroxides. Reductive dissolution

also releases Fe–P. Yet, as the model simulation shows (Fig. 4g, solid curves), the TPO_4 profiles are not reproduced using literature P : Fe ratios of $\varepsilon = 0.1$ (Slomp et al., 1996; Anschutz et al., 1998). The integrated TPO_4 concentration contained within the November peak is 2.5 times as high as the Fe^{2+} peak, implying that $\varepsilon \approx 2.5$. There is obviously a much more significant source of TPO_4 than the fraction which can be reasonably explained as Fe–P. We were unable to simulate the TPO_4 peak assuming enhanced release of Fe-P or preferential mineralization of organic P (not shown). In fact, our simulations point toward an intense yet ephemeral source of TPO_4 in the upper 5 cm when O_2 concentrations fall below 10 µM.

4.4 Massive phosphate release by *Beggiatoa ?*

Luxury uptake and release of TPO_4 under oscillating redox conditions by the giant sulfide oxidizing bacteria *Beggiatoa* and *Thiomargarita* has been reported (Schulz and Schulz, 2005; Brock and Schulz-Vogt, 2011; Goldhammer et al., 2010). These microorganisms convert porewater phosphate into intracellular polyphosphate granules under oxic conditions. Under anoxic conditions these compounds are hydrolyzed to release energy as well as TPO_4 to the surrounding porewater (Sannigrahi and Ingall, 2005; Schulz and Schulz, 2005; Brock and Schulz-Vogt, 2011). The metabolic stimulus and motive for phosphate release is poorly understood and beyond the scope of this study. Some laboratory studies indicate that polyphosphate breakdown may be part of an auxiliary metabolism arising from increased exposure to sulfide due to higher rates of sulfate reduction (Brock and Schulz-Vogt, 2011). Considering that *Beggiatoa* filaments were observed in great abundance during hypoxia in Boknis Eck, it seems reasonable to consider the possibility that the TPO_4 peak in October/November may be driven by these bacteria in addition to the release of Fe–P and organic P. Ingall and Jahnke (1994) and others (e.g. Boström et al., 1988; Sannigrahi and Ingall, 2005; Hupfer and Lewandowski, 2008) noted early on that TPO_4 released from iron oxyhydroxides and organic P under low oxygen conditions could only account for a fraction of the total rate of TPO_4 regeneration in sediments, and ascribed the rest to TPO_4 release by

Title Page

Abstract | Introduction

Conclusions | References

Tables | Figures

|◀ | ▶|

◀ | ▶

Back | Close

Full Screen / Esc

Printer-friendly Version

Interactive Discussion

microorganisms. More generally, microorganisms are believed to play a major role in benthic phosphorus cycling (Gächter and Meyer, 1993; Hupfer et al., 2004).

To test this idea, we modified the model to include intracellular P as a new dynamic variable (Fig. 1). The basic premise is that luxury uptake of TPO_4 from the porewater by *Beggiatoa* takes place during periods of oxygenated bottom waters, whereas net release of intracellular P to the porewater as TPO_4 occurs during hypoxia. Although *Beggiatoa* could conceivably take up TPO_4 directly from the bottom water by extension of their filaments through the diffusive boundary layer, it seems more plausible that they instead capitalize on the porewater TPO_4 pool where concentrations are at least an order-of-magnitude higher. Thus, if *Beggiatoa* can be considered as viable candidates for enhanced phosphorus cycling in Boknis Eck, then the TPO_4 added to the porewater in the uppermost sediment layers by mineralization processes over the year has to be sufficient to sustain the TPO_4 peak when taken up by the bacteria and then released again in autumn.

As a minimum requirement, we assumed that microbial phosphate uptake (P_{up}, My^{-1}) and release (P_{rel}, My^{-1}) only occurs if the *Beggiatoa* are active. This was achieved by making P_{up} and P_{rel} dependent on the rate of DNRA:

$$P_{up} = \chi_{up} \cdot R_{DNRA} \cdot \frac{[TPO_4]}{[TPO_4] + K_{TPO_4}} \cdot \frac{[O_2']}{[O_2'] + K_{O_2'}^P} \quad (7)$$

$$P_{rel} = \chi_{rel} \cdot R_{DNRA} \cdot \frac{[TPO_4]_{bac}}{[TPO_4]_{bac} + K_{TPO_4}^{bac}} \cdot \frac{K_{O_2'}^P}{[O_2'] + K_{O_2'}^P} \quad (8)$$

where $[TPO_4]_{bac}$ is the intracellular phosphate concentration and K_{TPO_4} and $K_{TPO_4}^{bac}$ are kinetic constants for phosphate uptake and release. These constants are assigned a value of $10\,\mu M$ to ensure uptake and release of TPO_4 at the low porewater concentrations observed. Because these processes relate to *Beggiatoa*, they employ the time-lagged O_2 concentration, O_2', in the same way as bacterial nitrate transport (Fig. 2d).

Benthic fluxes in seasonally-hypoxic sediments

A. W. Dale et al.

Title Page

Abstract | Introduction

Conclusions | References

Tables | Figures

◀ | ▶▶

◀ | ▶

Back | Close

Full Screen / Esc

Printer-friendly Version

Interactive Discussion

The oxygen limiting term includes the half-saturation constant $K_{O_2}^P$, which determines the concentration at which *Beggiatoa* become net releasers or assimilators of TPO_4. The rates are mostly sensitive to this parameter, and a value of $0.8\,\mu M$ best describes the data. χ_{up} and χ_{rel} are dimensionless parameters equal to 10 and 100, respectively, that simply decouple intracellular nitrate and phosphate dynamics and allow for a faster rate of intracellular TPO_4 release during hypoxia.

Model simulations considering an intracellular P pool provide a much better correspondence with the TPO_4 concentrations in November, but there is no improvement in October (Fig. 4g, dashed lines). However, since the rates of P uptake and release are sensitive to O_2 concentration, the October TPO_4 peak can be simulated by allowing for a faster rate of O_2 decrease between the August and September than the linear interpolation used in Fig. 2c (not shown). The simulations would therefore benefit from a higher sampling resolution of bottom water O_2 during this time of year. Because bioirrigation at the beginning of the year flushes out most of the dissolved TPO_4, our data are presently insufficient to identify additional TPO_4 sinks such as authigenic apatite precipitation or reversible adsorption onto iron mineral phases (Froelich et al., 1988; Ruttenburg and Berner, 1993; Goldhammer et al., 2010; Slomp et al., 1996, 1998).

The model reproduces the TPO_4 diffusive effluxes that accompany the peaks in October and November, with maximum fluxes of $1.2\,\mathrm{mmol\,m^{-2}\,d^{-1}}$ (Fig. 5). This maintains low C/P regeneration ratios of >20 even though bottom waters return to high levels (Fig. 7). Phosphate release rates of 0.8 and $0.6\,\mathrm{mmol\,m^{-2}\,d^{-1}}$ have been reported for the seasonally-hypoxic Arkona Basin and Bay of Concepción (Holmkvist et al., 2010; Mort et al., 2010). Benthic fluxes reported for quasi-permanent hypoxic shelf regions are at least an order of magnitude lower, including California borderland basins (Berelson et al., 1987; Jahnke, 1990; McManus et al., 1997) and the Washington and Oregon margins (Devol and Christensen, 1993; Severmann et al., 2010). At the highly productive Peruvian oxygen minimum zone, phosphate fluxes are higher at $0.4\,\mathrm{mmol\,m^{-2}\,d^{-1}}$. In general, it is the oscillation between oxic and hypoxic/anoxic conditions rather than permanent anoxic conditions that favors periods of short but

Benthic fluxes in seasonally-hypoxic sediments

A. W. Dale et al.

Title Page

Abstract	Introduction
Conclusions	References
Tables	Figures

◄ | ►|

◄ | ►

Back | Close

Full Screen / Esc

Printer-friendly Version

Interactive Discussion

intense bursts of phosphate release to the water column (Balzar et al., 1983; Koop et al., 1990; Cowan and Boynton, 1996; Mort et al., 2010). In this sense, *Beggiatoa* and/or iron-associated P may act as phosphorus capacitors in systems with oscillating redox conditions, releasing large amounts of TPO_4 in a short space of time and dramatically increasing the internal loading of TPO_4 in overlying waters.

The pulsed release of TPO_4 by *Beggiatoa* dominates the benthic P budget (Table 4). Maximum phosphate release rates of ca. $30\,nmol\,cm^{-3}\,d^{-1}$ are required to produce the November peak (Fig. 8) with depth-integrated rates of up to $4.5\,mmol\,m^{-2}\,d^{-1}$ (Fig. 6d). This is about 10 times larger than the flux of phosphate supplied by Fe–P and organic P combined (Fig. 6d). A similarly sized TPO_4 peak of $250\,\mu M$ measured in Namibian shelf sediments inhabited by *Thiomargarita* was explained by phosphate release rates of $500–1700\,nmol\,cm^3\,d^{-1}$ (Schulz and Schulz, 2005). The bacteria need only relatively low TPO_4 assimilation rates of $0.2\,mmol\,m^{-2}\,d^{-1}$ during winter and spring to accumulate enough phosphate to sustain the autumn release (not shown). This could be easily supplied by the phosphate released from organic P and Fe–P (Fig. 6d, Table 4). For comparison, depth-integrated phosphate uptake rates of 0.3 to $1.2\,mmol\,m^{-2}\,d^{-1}$ have been reported for anoxic laboratory incubations using *Beggitaota* and *Thiomargarita* (Goldhammer et al., 2010). Our model predicted rates are thus very much in agreement with the few data available on P cycling by giant sulfide oxidizers and provide more evidence for a significant role of these microorganisms in moderating P fluxes in seasonally hypoxic settings.

5 Conclusions

This study presents a time-series of porewater data from a seasonally-hypoxic coastal setting which is analyzed using a numerical model to quantify benthic processes and fluxes. Clear transient signals in the data are interpreted as changes in both reaction rates and transport processes (mainly bioirrigation and bubble irrigation). The model

Title Page

Abstract | Introduction

Conclusions | References

Tables | Figures

⏮ | ⏭

◄ | ►

Back | Close

Full Screen / Esc

Printer-friendly Version

Interactive Discussion

Benthic fluxes in seasonally-hypoxic sediments

A. W. Dale et al.

has led to new ideas concerning nutrient cycling in Boknis Eck sediments which may be more widely applicable.

Firstly, we have shown that solute exchange between the sediments and the water column is dominated by bioirrigation in winter and spring and by bubble-induced irrigation at irregular intervals from late spring to autumn. Molecular diffusion is important for highly reactive species such as O_2 and NO_3^-. Secondly, a very large transient peak in TPO_4 in excess of 400 µM develops in subsurface sediments at the end of the hypoxic period in October, leading to an extreme enrichment of P relative to C in the fluxes to the overlying water column. This feature is driven by a large pulsed release of TPO_4 to the porewater within a short space of time (∼ weeks). Based on published field evidence and laboratory experiments, we were able to reproduce this peak using new kinetic expressions that allow the giant sulfide-oxidizing bacteria *Beggiatoa* to take up TPO_4 during periods of oxic bottom waters and release TPO_4 when oxygen drops to low levels (∼10 µM). This does not require an external source of TPO_4 and agrees with the known distribution of *Beggiatoa* in these sediments and their ecology. Alternative sources of TPO_4, such as from Fe–P and organic P, do not provide a satisfactory simulation of the data at this stage, but cannot be ruled out indefinitely.

Further work is required to substantiate our findings. Although there are several pieces of circumstantial evidence in support of pseudo-irrigation by gas bubble transport, this has yet to be shown experimentally. Given the apparently episodic nature of gas eruption, continuous monitoring of gas escape and sediment porewater would be needed to capture these events and corroborate the hypothesis unless an alternative mechanistic explanation can be proposed. Bubble irrigation may be more common than currently presumed and is likely to be overlooked if sediments are sampled at a single time rather than as part of a time series study. Our suggestion that *Beggiatoa* are releasing TPO_4 would be strengthened with data on the temporal variability of the fraction of phosphate bound to iron oxyhydroxides as well as intra-cellular P concentrations. Sampling at bi-weekly intervals with additional support from benthic chamber deployments during the hypoxic period would also help to refine future modeling work.

The limitation of the 1-D model approach in not being able to simulate iron precipitation and dissolution on the walls of animal burrows is an additional aspect which will be addressed in future.

The strength of this study lies in the quantification of transient fluxes and process rates that are supported by a set of temporally resolved benthic data. We demonstrate that the accurate nutrient budgeting in muddy coastal sediments requires a careful consideration of temporal dynamics. Nevertheless, there are very few published modeling studies that explore seasonal benthic cycling which are constrained using data collected at sampling frequencies adequate to capture the transient dynamics (e.g. Aller, 1977; Fossing et al., 2004; Klump and Martens, 1989). This is especially true for phosphorus dynamics in seasonally hypoxic or anoxic systems with pronounced redox oscillations. These sediments may behave as phosphate capacitors, whereby particulates (e.g. iron oxyhydroxides and/or bacteria) are charged with TPO_4 during oxic conditions and then discharge TPO_4 when hypoxia is established. More studies in environments such as Boknis Eck could prove invaluable to better constrain the kinetics of key reactions and improve the predictive power of basin scale models of systems with seasonal or episodic hypoxia such as the Baltic Sea (e.g. Eilola et al., 2011).

Supplementary material related to this article is available online at: http://www.biogeosciences-discuss.net/9/11517/2012/ bgd-9-11517-2012-supplement.pdf.

Eck Time Series station is run by the Marine Biogeochemistry research division at GEOMAR (http://www.ifm-geomar.de/index.php?id=bokniseck).

References

Abegg, F. and Anderson, A. L.: The acoustic turbid layer in muddy sediments of Eckernfoerde Bay, Western Baltic: methane concentration, saturation and bubble characteristics, Mar. Geol., 137, 137–147, 1997.

Algar, C. K., Boudreau, B. P., and Barry, M. A.: Initial rise of bubbles in cohesive sediments by a process of viscoelastic fracture, J. Geophys. Res., 116, B04207, doi:10.1029/2010JB008133, 2011.

Aller, R. C.: The influence of macrobenthos on chemical diagenesis of marine sediments, Ph.D. dissertation, Yale University, 1977.

Aller, R. C. and Aller, J. Y.: The effect of biogenic irrigation intensity and solute exchange on diagenetic reaction rates in marine sediments, J. Mar. Res., 56, 905–936, 1998.

Anschutz, P., Zhong, S., and Sundby, B.: Burial efficiency of phosphorus and the geochemistry of iron in continental margin sediments, Limnol. Oceanogr., 43, 53–64, 1998.

Arntz, W. E.: Zonation and dynamics of macrobenthos biomass in an area stressed by oxygen deficiency, in: Stress Effects on Natural Ecosystems, edited by: Barret, G. W. and Rosenberg, R., Wiley, New York, 215–226, 1981.

Arntz, W. E. and Rumohr, H.: An experimental study of macrobenthic colonization and succession, and the importance of seasonal variation in temperate latitudes, J. Exp. Mar. Biol. Ecol., 64, 17–45, 1982.

Balzer, W.: On the distribution of iron and manganese at the sediment/water interface: thermodynamic versus kinetic control, Geochim. Cosmochim. Ac., 46, 1153–1161, 1982.

Balzer, W., Grasshoff, K., Dieckmann, P., Haardt, H., and Petersohn, U.: Redox turnover at the sediment/water interface studied in a large bell jar system, Oceanol. Acta, 6, 337–344, 1983.

Balzer, W., Pollehne, F., and Erlenkeuser, H.: Cycling of organic carbon in a coastal marine system, in: Sly, P. G., Sediments and Water Interactions, Springer Verlag, New York, 325–330, 1986.

Balzer, W., Erlenkeuser, H., Hartmann, P. J., Müller, P. J., and Pollehne, F.: Diagenesis and exchange processes at the benthic boundary, in: Seawater-Sediment Interactions in Coastal

Benthic fluxes in seasonally-hypoxic sediments

A. W. Dale et al.

Waters. An Interdisciplinary Approach, edited by: Rumohr, J., Wlager, E., and Zeitzschel, B., Springer-Verlag, Berlin Heidelberg, 111–161, 1987.

Bange, H. W., Bergmann, K., Hansen, H. P., Kock, A., Koppe, R., Malien, F., and Ostrau, C.: Dissolved methane during hypoxic events at the Boknis Eck time series station (Eckernförde Bay, SW Baltic Sea), Biogeosciences, 7, 1279–1284, doi:10.5194/bg-7-1279-2010, 2010.

Bange, H. W., Hansen, H. P., Karstensen, J., Malien, F., Petereit, C., Laß, K., and Friedrichs, G., Dale, A.: Boknis Eck Time Series Station: easurements from 1957 to 2010, LOICZ Inprint., 1, 16–22, 2011.

Berelson, W. M., Hammond, D. E., and Johnson, K. S.: Benthic fluxes and the cycling of biogenic silica and carbon in two Southern California borderland basins, Geochim. Cosmochim. Ac., 51, 1345–1363, 1987.

Berg, P., Rysgaard, S., and Thamdrup, B.: Dynamic modeling of early diagenesis and nutrient cycling. A case study in an Arctic marine sediment, Am. J. Sci., 303, 905–955, 2003.

Berner, R. A.: Early Diagenesis: a Theoretical Approach, Princeton University Press, Princeton, 241 pp., 1980.

Bertics, V. J., Löscher, C. R., Salonen, I., Dale, A. W., Schmitz, R. A., and Treude, T.: Occurrence of benthic microbial nitrogen fixation coupled to sulfate reduction in the seasonally hypoxic Eckernförde Bay, Baltic Sea, Biogeosciences Discuss., 9, 6489–6533, doi:10.5194/bgd-9-6489-2012, 2012.

Bohlen, L., Dale, A. W., Sommer, S., Mosch, T., Hensen, C., Noffke, A., Scholz, F., and Wallmann, K.: Benthic nitrogen cycling traversing the Peruvian oxygen minimum zone, Geochim. Cosmochim. Ac., 75, 6094–6111, 2011.

Boudreau, B. P.: On the equivalence of nonlocal and radial-diffusion models for porewater irrigation, J. Mar. Res., 42, 731–735, 1984.

Boudreau, B. P.: A method-of-lines code for carbon and nutrient diagenesis in aquatic sediments, Comput. Geosci., 22, 479–496, 1996.

Boudreau, B. P.: Diagenetic Models and Their Implementation: Modelling Transport and Reactions in Aquatic Sediments, Springer-Verlag, Berlin, 414 pp., 1997.

Boudreau, B. P. and Marinelli, R. L.: A modelling study of discontinuous biological irrigation, J. Mar. Res., 52, 947–968, 1994.

Briggs, B. R., Pohlman, J. W., Torres, M., Riedel, M., Brodie, E. L., and Colwell, F. S.: Macroscopic biofilms in fracture-dominated sediment thatanaerobically oxidize methane, Appl. Environ. Microb., 77, 6780–6787, 2011.

Title Page

Abstract | Introduction

Conclusions | References

Tables | Figures

⏮ | ⏭

◀ | ▶

Back | Close

Full Screen / Esc

Printer-friendly Version

Interactive Discussion

Brock, J. and Schulz-Vogt, H. N.: Sulfide induces phosphate release from polyphosphate in cultures of a marine Beggiatoa strain, ISME J., 5, 497–506, 2010.

Conley, D. J. and Johnstone, R. W.: Biogeochemistry of N, P and Si in Baltic Sea sediments: response to a simulated deposition of a spring diatom bloom, Mar. Ecol.-Prog. Ser., 122, 265–276, 1995.

Conley, D. J., Humborg, C., Rahm, L., Savchuk, O. P., and Wulff, F.: Hypoxia in the Baltic Sea and basin-scale changes in phosphorus biogeochemistry, Envir. Sci. Tech. Lib., 36, 5315–5320, 2002.

Cowan, J. L. W. and Boynton, W. R.: Sediment-water oxygen and nutrient exchanges along the longitudinal axis of Chesapeake Bay: seasonal patterns, controlling factors and ecological significance, Estuaries, 19, 562–580, 1996.

Dale, A. W., Van Cappellen, P., Aguilera, D. R., and Regnier, P.: Methane efflux from marine sediments in passive and active margins: estimations from bioenergetic reaction-transport simulations, Earth Planet. Sc. Lett., 265, 329–344, 2008.

Dale, A. W., Brüchert, V., Alperin, M., and Regnier, P.: An integrated sulfur isotope model for Namibian shelf sediments, Geochim. Cosmochim. Ac., 73, 1924–1944, 2009a.

Dale, A. W., Regnier, P., Van Cappellen, P., Fossing, H., Jensen, J. B., and Jorgensen, B. B.: Remote quantification of methane fluxes in gassy marine sediments through seismic survey, Geology, 37, 235–238, 2009b.

Dale, A. W., Sommer, S., Bohlen, L., Treude, T., Bertics, V. J., Bange, H. W., Pfannkuche, O., Schorp, T., Mattsdotter, M., and Wallmann, K.: Rates and regulation of nitrogen cycling in seasonally hypoxic sediments during winter (Boknis Eck, SW Baltic Sea): sensitivity to environmental variables, Estuar. Coast. Shelf S., 95, 14–28, 2011.

Dale, A. W., Meyers, S. R., Aguilera, D. R., Arndt, S., and Wallmann, K.: Processes controlling organic carbon and molybdenum accumulation rates in Cretaceous marine sediments from the Cenomanian-Turonian interval including Oceanic Anoxic Event 2. Chem. Geol., doi:10.1016/j.chemgeo.2011.10.004, 2012.

Devol, A. H. and Christensen, J. P.: Benthic fluxes and nitrogen cycling in sediments of the continental margin of the Eastern North Pacific, J. Mar. Res., 51, 345–372, 1993.

Diaz, R. J. and Rosenberg, R.: Spreading dead zones and consequences for marine ecosystems, Science, 321, 926–929, doi:10.1126/science.1156401, 2008.

Benthic fluxes in seasonally-hypoxic sediments

A. W. Dale et al.

Title Page

Abstract	Introduction
Conclusions	References
Tables	Figures

◀ ▶

◀ ▶

Back Close

Full Screen / Esc

Printer-friendly Version

Interactive Discussion

Duan, Z., Moller, N., Greenberg, J., and Weare, J. H.: The prediction of methane solubility in natural waters to high ionic strength from 0° to 250° and from 0 to 1600 bar, Geochim. Cosmochim. Ac., 56, 1451–1460, 1992.

Ehrhardt, M. and Wenck, A.: Wind pattern and hydrogen sulfide in shallow waters of the Western Baltic Sea, a cause effect relationship?, Meeresforschung, 30, 101–110, 1984.

Eilola, K., Gustafsson, B. G., Kuznetsok, I., Meier, H. E. M., Neumann, T., and Savchuk, O. P.: Evaluation of biogeochemical cycles in an ensemble of three state-of-the-art numerical models of the Baltic Sea, J. Marine Syst., 88, 267–284, 2011.

Emerson, S., Jahnke, R., and Heggie, D.: Sediment-water exchange in shallow water estuarine sediments, J. Mar. Res., 42, 709–730, 1984.

Forster, S., Glud, R. N., Gundersen, J. K., and Huettel, M.: In situ study of bromide tracer and oxygen flux in coastal sediments, Estuar. Coast. Shelf S., 49, 813–827, 1999.

Forster, S., Khalili, A., and Kitlar, J.: Variation of nonlocal irrigation in a subtidal benthic community, J. Mar. Res., 61, 335–357, 2003.

Fossing, H., Berg, P., Thamdrup, B., Rysgaard, S., Sorensen, H. M., and Nielsen, K.: A model set-up for an oxygen and nutrient flux model for Aarhus Bay (Denmark), Technical Report, No. 483, National Environmental Research Institute (NERI), 68 pp. 2004.

Froelich, P. N., Klinkhammer, G. P., Bender, M. L., Luedtke, N. A., Heath, G. R., Cullen, D., and Dauphin, P.: Early oxidation of organic matter in pelagic sediments of the Eastern Equatorial Atlantic: suboxic diagenesis, Geochim. Cosmochim. Ac., 43, 1075–1090, 1979.

Froelich, P., Arthur, M. A., Burnett, W. C., Deakin, M., Hensley, V., Jahnke, R., Kaul, N., Kim, K. H., Roe, K., Soutar, A., and Vathakanon, C.: Early diagenesis of organic matter in Peru continental margin sediments: phosphorite precipitation, Mar. Geol., 80, 309–343, 1988.

Gachter, R. and Meyer, J. S.: The role of microorganisms in mobilization and fixation of phosphorus in sediments, Hydrobiologia, 253, 103–121, 1993.

Glud, R. N., Gundersen, J. K., Jorgensen, B. B., Revsbech, N. P., and Schulz, H. D.: Diffusive and total oxygen uptake of deep-sea sediments in the Eastern South Atlantic Ocean: in situ and laboratory measurements, Deep-Sea Res. Pt. II, 41, 1767–1788, 1994.

Goldhammer, T., Brüchert, V., Ferdelman, T. G., and Zabel, M.: Microbial sequestration of phosphorus in anoxic upwelling sediments, Nat. Geosci., 3, 557–561, 2010.

Title Page

Abstract | Introduction

Conclusions | References

Tables | Figures

◀ | ▶

◀ | ▶

Back | Close

Full Screen / Esc

Printer-friendly Version

Interactive Discussion

Graf, G., Bengtsson, W., Diesner, U., Schulz, R., and Theede, H.: Benthic response to sedimentation of a spring phytoplankton bloom: process and budget, Mar. Biol., 245, 201–208, 1982.

Graf, G., Schulz, R., Peinert, R., and Meyer-Reil, L. A.: Benthic response to sedimentation events during autumn to spring at a shallow-water station in the Western Kiel Bight, Mar. Biol., 77, 235–246, 1983.

Haeckel, M., Boudreau, B. P., and Wallmann, K.: Bubble-induced porewater mixing: a 3-D model for deep porewater irrigation, Geochim. Cosmochim. Ac., 71, 5135–5154, 2007.

Haese, R. R.: The biogeochemistry of iron, in: Marine Geochemistry, 2nd edn., edited by: Schulz, H. D. and Zabel, M., Springer-Verlag, Berlin, 241–270, 2006.

Haese, R. R., Wallmann, K., Kretzmann, U., Müller, P. J., and Schulz, H. D.: Iron species determination to investigate the early diagenetic reactivity in marine sediments, Geochim. Cosmochim. Ac., 61, 63–72, 1997.

Hansen, H. P., Giesenhagen, H. C., and Behrends, G.: Seasonal and long-term control of bottom water oxygen deficiency in a stratified shallow-coastal system, ICES J. Mar. Sci., 56 Supplement, 65–71, 1999.

HELCOM: Eutrophication in the Baltic Sea – an Integrated Thematic Assessment of the Effects of Nutrient Enrichment and Eutrophication in the Baltic Sea Region, Balt. Sea Environ. Proc. No. 115B, 2009.

Holmkvist, L., Arning, E. T., Küster-Heins, K., Vandieken, V., Peckmann, J., Zabel, M., and Jørgensen, B. B.: Phosphate geochemistry, mineralization processes, and *Thioploca* distribution in shelf sediments off Central Chile, Mar. Geol., 277, 61–72, 2010.

Hupfer, M. and Lewandowski, J.: Oxygen controls the phosphorus release from lake sediments – a long-lasting paradigm in limnology, Int. Rev. Hydrobiol., 92, 415–432, 2008.

Ingall, E. and Jahnke, R.: Evidence for enhanced phosphorus regeneration from marine sediments overlain by oxygen depleted waters, Geochim. Cosmochim. Ac., 58, 2571–2575, 1994.

Ingall, E. and Jahnke, R.: Influence of water-column anoxia on the elemental fractionation of carbon and phosphorus during sediment diagenesis, Mar. Geol., 139, 219–229, 1997.

Jackson, D. R., Williams, K. L., Wever, T. F., Friedrichs, C. T., and Wright, L. D.: Sonar evidence for methane ebullition in Eckernförde Bay, Cont. Shelf Res., 18, 1893–1915, 1998.

Jahnke, R. A.: Early diagenesis and recycling of biogenic debris at the seafloor, Santa Monica Basin, California, J. Mar. Res., 48, 413–436, 1990.

Benthic fluxes in seasonally-hypoxic sediments

A. W. Dale et al.

Jensen, J. B. and Bennike, O.: Geological setting as background for methane distribution in Holocene mud deposits, Århus Bay, Denmark, Cont. Shelf Res., 29, 775–784, 2009.

Jourabchi, P., Van Cappellen, P., and Regnier, P.: Quantitative interpretation of pH distributions in aquatic sediments: a reaction-transport modeling approach, Am. J. Sci., 305, 919–956. 2005.

Klump, J. V. and Martens, C. S.: Biogeochemical cycling in an organic rich coastal marine basin – II. Nutrient sediment-water exchange processes, Geochim. Cosmochim. Ac., 45, 101–121, 1981.

Klump, J. V. and Martens, C. S.: The seasonality of nutrient regeneration in an organic-rich coastal sediment: kinetic modeling of changing pore-water nutrient and sulfate distributions, Limnol. Oceanogr., 34, 559–577, 1989.

Koop, K., Boynton, W. R., Wulff, F., and Carman, R.: Sediment-water oxygen and nutrient exchanges along a depth gradient in the Baltic Sea, Mar. Ecol.-Prog. Ser., 63, 65–77, 1990.

Krom, M. D. and Berner, R. A.: The diagenesis of phosphorus in a nearshore marine sediment, Geochim. Cosmochim. Ac., 45, 207–216, 1981.

Lapp, B. and Balzer, W.: Early diagenesis of trace metals used as an indicator of past productivity changes in coastal sediments, Geochim. Cosmochim. Ac., 57, 4639–4652, 1993.

Levin, L. A., Ekau, W., Gooday, A. J., Jorissen, F., Middelburg, J. J., Naqvi, S. W. A., Neira, C., Rabalais, N. N., and Zhang, J.: Effects of natural and human-induced hypoxia on coastal benthos, Biogeosciences, 6, 2063–2098, doi:10.5194/bg-6-2063-2009, 2009.

Lewandowski, J., Laskov, C., and Hupfer, M.: The relationship between *Chironomus plumosus* burrows and the spatial distribution of pore-water phosphate, iron and ammonium in lake sediments, Freshwater Biol., 52, 331–343, 2007.

Matens, C. S.: Control of methane sediment-water bubble transport by macroinfaunal irrigation in Cape Lookout Bight, North Carolina, Science, 192, 998–1000, 1976.

Martens, C. S. and Klump, J. V.: Biogeochemical cycling in an organic-rich coastal marine basin – I. Methane sediment-water exchange processes, Geochim. Cosmochim. Ac., 44, 471–490, 1980.

Martens, C. S., Albert, D. B., and Alperin, M. J.: Biogeochemical processes controlling methane in gassy coastal sediments – Part 1. A model coupling organic matter flux to gas production, oxidation and transport, Cont. Shelf Res., 18, 1741–1770, 1998.

Martin, W. R. and Banta, G. T.: The measurement of sediment irrigation rates: a comparison of the Br- tracer and 222Rn/226Ra disequilibrium techniques, J. Mar. Res., 50, 125–154, 1992.

Benthic fluxes in seasonally-hypoxic sediments

A. W. Dale et al.

Title Page

Abstract | Introduction

Conclusions | References

Tables | Figures

Back | Close

Full Screen / Esc

Printer-friendly Version

Interactive Discussion

McManus, J., Berelson, W. M., Coale, K. H., Johnson, K. S., and Kilgore, T. E.: Phosphorus regeneration in continental margin sediments, Geochim. Cosmochim. Ac., 61, 2891–2907, 1997.

Meile, C., Berg, P., Van Cappellen, P., and Tuncay, K.: Solute-specific pore water irrigation: implications for chemical cycling in early diagenesis, J. Mar. Res., 64, 601–621, 2005.

Meyer-Reil, L. A.: Benthic response to sedimentation events during autumn to spring at a shallow water station in the Western Kiel Bight, Mar. Biol., 77, 247–256, 1983.

Meysman, F. J. R., Galaktionov, O. S., Gribsholt, B., and Middelburg, J. J.: Bio-irrigation in permeable sediments: an assessment of model complexity, J. Mar. Res., 64, 589–627, 2006.

Middelburg, J. J. and Levin, L. A.: Coastal hypoxia and sediment biogeochemistry, Biogeosciences, 6, 1273–1293, doi:10.5194/bg-6-1273-2009, 2009.

Middelburg, J. J., Soetaert, K., Herman, P. M. J., and Heip, C. H. R.: Denitrification in marine sediments: a model study, Global Biogeochem. Cy., 10, 661–673, 1996.

Mogollón, J. M., Dale, A. W., Fossing, H., and Regnier, P.: Timescales for the development of methanogenesis and free gas layers in recently-deposited sediments of Arkona Basin (Baltic Sea), Biogeosciences, 9, 1915–1933, doi:10.5194/bg-9-1915-2012, 2012.

Mort, H. P., Slomp, C. P., Gustafsson, B. G., and Andersen, T. J.: Phosphorus recycling and burial in Baltic Sea sediments with contrasting redox conditions, Geochim. Cosmochim. Ac., 74, 1350–1362, 2010.

Orsi, T. H., Werner, F., Milkert, D., Anderson, A. L., and Bryant, W. R.: Environmental overview of Eckernförde Bay, Northern Germany. Geo-Mar. Lett., 16, 140–147, 1996.

Pakhomova, S. V., Hall, P. O. J., Kononets, M. Y., Rozanov, A. G., Tengberg, A., and Vershinin, A. V.: Fluxes of iron and manganese across the sediment-water interface under various redox conditions, Mar. Chem., 107, 319–331, 2007.

Postma, D.: Pyrite and siderite formation in brackish and freshwater swamp sediments, Am. J. Sci., 282, 1151–1183, 1982.

Poulton, S. W.: Sulfide oxidation and iron dissolution kinetics during the reaction of dissolved sulfide with ferrihydrite, Chem. Geol., 202, 79–94, 2003.

Preisler, A., de Beer, D., Lichtschlag, A., Lavik, G., Boetius, A., and Jørgensen, B. B.: Biological and chemical sulfide oxidation in a *Beggiatoa* inhabited marine sediment, ISME J., 1, 341–353, 2007.

Rao, A. M. F. and Jahnke, R. A.: Quantifying pore water exchange across the sediment-water interface in the deep sea with in situ tracer studies, Limnol. Oceanogr.-Meth., 2, 75–90, 2004.

Title Page

Abstract | Introduction

Conclusions | References

Tables | Figures

◀ | ▶

◀ | ▶

Back | Close

Full Screen / Esc

Printer-friendly Version

Interactive Discussion

Ray, A. J. and Aller, R. C.: Physical irrigation of relict burrows: implications for sediment chemistry, Mar. Geol., 62, 371–379, 1985.

Reed, D. C., Slomp, C. P., and Gustafsson, B. G.: Sedimentary phosphorus dynamics and the evolution of bottom-water hypoxia: a coupled benthic-pelagic model of a coastal system, Limnol. Oceanogr., 56, 1075–1092. 2011.

Rozan, T. F., Taillefert, M., Trouwborst, R. E., Glazer, B. T., Ma, S. F., Herszage, J., Valdes, L. M., Price, K. S., and Luther, G. W.: Iron-sulfur-phosphorus cycling in the sediments of a shallow coastal bay: implications for sediment nutrient release and benthic macroalgal blooms, Limnol. Oceanogr., 47, 1346–1354, 2002.

Ruttenberg, K. C. and Berner, R. A.: Authigenic apatite formation and burial in sediments from non-upwelling, continental margin environments, Geochim. Cosmochim. Ac., 57, 991–1007, 1993.

Sannigrahi, P. and Ingall, E.: Polyphosphates as a source of enhanced P fluxes in marine sediments overlain by anoxic waters: evidence from 31P NMR, Geochem. T., 6, 52, 2005.

Sayles, F. L. and Martin, W. R.: In situ tracer studies of solute transport across the sediment-water interface at the Bermuda Time Series site, Deep-Sea Res., 42, 31–52, 1995.

Schlüter, M., Sauter, E., Hansen, H. P., and Suess, E.: Seasonal variations of bioirrigation in coastal sediments: modelling of field data, Geochim. Cosmochim. Ac., 64, 821–834, 2000.

Schulz, H. D.: Quantification of early diagenesis: dissolved constituents in pore water and signals in the solid phase, in: Marine Geochemistry, 2nd edn., edited by: Schulz, H. D. and Zabel, M., Springer-Verlag, Berlin, 73–124, 2006.

Schulz, H. N. and Schulz, H. D.: Large sulfur bacteria and the formation of phosphorite, Science, 307, 416–418, 2005.

Schwalenberg, K., Haeckel, M., Poort, J., and Jegen, M.: Evaluation of gas hydrate deposits in an active seep area using marine controlled source electromagnetics: results from Opouawe Bank, Hikurangi Margin, New Zealand, Mar. Geol., 272, 79–88, 2010.

Severmann, S., McManus, J., Berelson, W. M., and Hammond, D. E.: The continental shelf benthic iron flux and its isotope composition, Geochim. Cosmochim. Ac., 74, 3984–4004, 2010.

Slomp, C. P., Epping, E. H. G., Helder, W., and Van Raaphorst, W.: A key role for iron-bound phosphorus in authigenic apatite formation in North Atlantic continental platform sediments, J. Mar. Res., 54, 1179–1205, 1996.

Benthic fluxes in seasonally-hypoxic sediments

A. W. Dale et al.

Title Page

Abstract | Introduction

Conclusions | References

Tables | Figures

◄ | ►|

◄ | ►

Back | Close

Full Screen / Esc

Printer-friendly Version

Interactive Discussion

Slomp, C. P., Malschaert, J. F. P., and Van Raaphorst, W.: The role of adsorption in sediment-water exchange of phosphate in North Sea continental margin sediments, Limnol. Oceanogr., 43, 832–846, 1998.

Smetacek, V., Bodungen, B. V., Bölterm, M., Bröckel, K. V., Dawson, R., Knoppers, B., Liebezeit, G., Martens, P., Peinert, P., Pollehne, F., Stegmann, P., Wolter, K., and Zeitzschel, B.: The pelagic system, in: Seawater-Sediment Interactions in Coastal Waters. An Interdisclipinary Approach, edited by: Rumohr, J., Wlager, E., and Zeitzschel, B., Springer-Verlag, Berlin Heidelberg, 32–56, 1987.

Sommer, S., Türk, M., Kriwanek, S., and Pfannkuche, O.: Gas exchange system for extended in situ benthic chamber flux measurements under controlled oxygen conditions: first application – sea bed methane emission measurements at Captain Arutyunov mud volcano, Limnol. Oceanogr.-Meth., 6, 23–33, 2008.

Sundby, B., Gobeil, C., Silverberg, N., and Mucci, A.: The phosphorus cycle in coastal marine sedmients, Limnol. Oceanogr., 37, 1129–1145, 1992.

Treude, T., Krüger, M., Boetius, A., and Jørgensen, B. B.: Environmental control on anaerobic oxidation of methane in the gassy sediments of Eckernförde Bay (German Baltic), Limnol. Oceanogr., 50, 1771–1786, 2005.

Wever, T. F. and Fiedler, H. M.: Variability of acoustic turbidity in Eckernförde Bay (southwest Baltic Sea) related to the annual temperature cycle, Mar. Geol., 125, 21–27, 1995.

Table 1. Sampling dates where multiple cores (MUC) were retrieved for geochemical analysis and bioirrigation experiments. Temperature, salinity and dissolved oxygen data in the bottom water (28 m) are also listed, along with the temperature-correction factor for reaction rates, $f(T)$.

Sampling no.	Date in 2010	Geochemistry	Bioirrigation	T (°C)	S (−)	O_2 (µM)	$f(T)^a$
1	18 Feb	3 × MUC	Yes	3.1	23.1	316	–
2	23 Feb	2 × MUC	No	0.16	15.9	359	–
3	4 Mar	–	Yes	0.26	17.9	334	1.0
4	22 Mar	2 × MUC	Yes	2.1	22.7	328	–
5	28 Apr	4 × MUC [b]	Yes	3.0	22.5	194	1.1
6	28 May	1 × MUC	Yes	3.8	21.5	141	1.2
7	1 Jul	2 × MUC	Yes	4.3	21.1	70	1.3
8	12 Aug	2 × MUC	Yes	8.8	24.2	47	2.1
9	9 Sep	2 × MUC	Yes	8.5	22.7	5	2.0
10	12 Oct	2 × MUC	Yes	10.4	21.6	2	2.5
11	17 Nov	2 × MUC	Yes	10.0	22.6	222	2.4
12	6 Dec	2 × MUC	Yes	6.5	22.6	263	1.6

[a] Formula for $f(T)$ is given in the Supplement.
[b] Two cores on 28 April were retrieved using a benthic lander.

Table 2. Table 2. Reaction network used in the biogeochemical model.

Rate	Stoichiometry[a,b,c]	Rate expression[d,e]	Unit[f]
POM mineralization reactions			
R_{O_2}	$G_i + O_2 \rightarrow TCO_2 + (N:C)_i NH_4^+ + (P:C)_i TPO_4$	$f(T) \cdot k_{Gi} \cdot f_{ox} \cdot G_i / f_{POC} \cdot f_{K-O_2}$	mmol cm^{-3} d^{-1} of TCO_2
R_{NO_3}	$G_i + 2NO_3^- \rightarrow 2NO_2^- + TCO_2 + (N:C)_i NH_4^+ + (P:C)_i TPO_4$	$f(T) \cdot k_{Gi} \cdot G_i / f_{POC} \cdot f_{K-NO_3} \cdot (1 - f_{K-O_2})$	mmol cm^{-3} d^{-1} of TCO_2
R_{NO_2}	$G_i + 1.33 NO_2^- \rightarrow 0.66 N_2 + TCO_2 + (N:C)_i NH_4^+ + (P:C)_i TPO_4$	$f(T) \cdot k_{Gi} \cdot G_i / f_{POC} \cdot f_{K-NO_2} \cdot (1 - f_{K-O_2})$	mmol cm^{-3} d^{-1} of TCO_2
R_{Fe}	$G_i + 4Fe(OH)_{3-A} + 4\theta_A(Fe-P)_A \rightarrow 4Fe^{2+} + TCO_2 + (N:C)_i NH_4^+ + (4\theta_A + (P:C)_i)TPO_4$	$f(T) \cdot k_{Gi} \cdot G_i / f_{POC} \cdot f_{K-Fe} \cdot (1 - f_{K-NO_3}) \cdot (1 - f_{K-NO_2}) \cdot (1 - f_{K-O_2})$	mmol cm^{-3} d^{-1} of TCO_2
R_{SO4}	$G_i + 0.5 SO_4^{2-} \rightarrow 0.5 TH_2S + TCO_2 + (N:C)_i NH_4^+ + (P:C)_i TPO_4$	$f(T) \cdot k_{Gi} \cdot G_i / f_{POC} \cdot f_{K-SO_4} \cdot (1 - f_{K-Fe}) \cdot (1 - f_{K-NO_3}) \cdot (1 - f_{K-NO_2}) \cdot (1 - f_{K-O_2})$	mmol cm^{-3} d^{-1} of TCO_2
R_{CH4}	$G_i \rightarrow 0.5 CH_4 + TCO_2 + (N:C)_i NH_4^+ + (P:C)_i TPO_4$	$f(T) \cdot k_{Gi} \cdot G_i / f_{POC} \cdot (1 - f_{K-SO_4}) \cdot (1 - f_{K-Fe}) \cdot (1 - f_{K-NO_3}) \cdot (1 - f_{K-NO_2}) \cdot (1 - f_{K-O_2})$	mmol cm^{-3} d^{-1} of TCO_2
Secondary redox reactions			
R_{DNRA}	$TH_2S + NO_{3\,bac}^- \rightarrow SO_4^{2-} + NH_4^+$	$f(T) \cdot k_{DNRA} \cdot NO_{3\,bac}^- \cdot TH_2S$	mmol cm^{-3} d^{-1} of NO_3^-
R_{amx}	$NH_4^+ + NO_2^- \rightarrow N_2$	$f(T) \cdot k_{amx} \cdot NO_2^- \cdot NH_4^+$	mmol cm^{-3} d^{-1} of N_2
R_{NH4ox}	$NH_4^+ + 1.5 O_2 \rightarrow NO_2^-$	$f(T) \cdot k_{NH4ox} \cdot O_2 \cdot NH_4^+$	mmol cm^{-3} d^{-1} of NH_4^+
R_{NO2ox}	$NO_2^- + 0.5 O_2 \rightarrow NO_3^-$	$f(T) \cdot k_{NO2ox} \cdot O_2 \cdot NO_2^-$	mmol cm^{-3} d^{-1} of NO_2^-
R_{AOM}	$CH_4 + SO_4^{2-} \rightarrow TH_2S^-$	$f(T) \cdot k_{AOM} \cdot CH_4 \cdot f_{SO_4}$	mmol cm^{-3} d^{-1} of CH_4
R_{H2Sox}	$TH_2S + 2O_2 \rightarrow SO_4^{2-}$	$f(T) \cdot k_{H2Sox} \cdot O_2 \cdot TH_2S$	mmol cm^{-3} d^{-1} of TH_2S
R_{Fe2ox}	$Fe^{2+} + 0.25 O_2 + \varepsilon \cdot TPO_4 \rightarrow Fe(OH)_{3-A} + \varepsilon \cdot Fe-P$	$f(T) \cdot k_{Fe2ox} \cdot O_2 \cdot Fe^{2+}$	mmol cm^{-3} d^{-1} of Fe^{2+}
	and rate of associated TPO$_4$ uptake =	$\varepsilon \cdot R_{Fe2ox} \cdot f_{K-TPO_4}$	mmol cm^{-3} d^{-1} of TPO_4
R_{FeS2ox}	$FeS_2 + 3.5 O_2 \rightarrow Fe^{2+} + 2SO_4^{2-}$	$f(T) \cdot k_{FeS2ox} \cdot O_2 \cdot FeS_2 / f_{Fe}$	mmol cm^{-3} d^{-1} of Fe^{2+}
R_{FeS2p}	$Fe^{2+} + 2TH_2S \rightarrow FeS_2 + H_2$	$f(T) \cdot k_{FeS_2p} \cdot Fe^{2+} \cdot TH_2S$	mmol cm^{-3} d^{-1} of Fe^{2+}
R_{Fe3red}	$(Fe(OH)_3)_i + \theta(Fe-P)_i + 1/8 TH_2S \rightarrow Fe^{2+} + 1/8 SO_4^{2-} + \theta_i TPO_4$	$f(T) \cdot k_{Fe3red} \cdot (Fe(OH)_3)_i \cdot TH_2S^{0.5} \cdot \frac{K_{O_2'}^{Fe}}{[O_2'] + K_{O_2'}^{Fe}} \cdot \frac{1}{f_{Fe}}$	mmol cm^{-3} d^{-1} of Fe^{2+}

[a] Rates of POM degradation are dependent on the specific organic matter pool, G_i, under consideration. POM is defined as $CN_{(N:C)_i} P_{(P:C)_i}$.

[b] For clarity, the reactions are not proton balanced and H_2O is omitted.

[c] TPO_4 release during DIR (R_{Fe}) and reductive iron dissolution (R_{Fe3red}) is calculated using the fraction of iron-associated TPO_4 (Fe–P) bound to $Fe(OH)_3$,
$\theta_i = \frac{[Fe-P]_i \cdot f_{Fe}}{[Fe(OH)_3]_i \cdot f_P}$ in mol P (mol Fe)$^{-1}$ where i corresponds to $Fe(OH)_3$ pool A or B (see text).

[d] Kinetic limiting terms: $f_{K-j} = \frac{[j]}{[j] + K_j}$ (for j = O_2, NO_2^-, NO_3^-, $Fe(OH)_3$, SO_4^{2-}, TPO_4), where K_j is the half-saturation constant for species j.

[e] Factors to convert between particulate and dissolved C, Fe and P (f_{POC}, f_{Fe}, and f_P) are given in the Supplement.

[f] Rate units for the other species can be determined by the reaction stoichiometry. A separate equation for TPO_4 is provided for R_{Fe2ox} (see text).

Table 3. Important parameters used in the biogeochemical model. Time-dependent parameters denoted "variable" are shown in Fig. 2. All other parameters are listed in the Supplement.

Parameter	Description	Value	Unit	Main constraint
T	Bottom water temperature	Variable	K	Measured (Dale et al., 2011)
S	Bottom water salinity	Variable [a]	1	Measured (Dale et al., 2011)
$v_a(0)$	Advection velocity for dissolved methane	Variable	$cm\,d^{-1}$	Measured SO_4^{2-} and TCO_2 profiles and SR rates (this study)
$D_b(0)$	Bioturbation coefficient at surface	Variable	$cm^2\,d^{-1}$	Assumed based on steady state model (Dale et al., 2011)
α_{bi1}	Bioirrigation coefficient	Variable	d^{-1}	Measured with Br^- incubations (this study)
α_{bi2}	Bioirrigation coefficient	Variable	cm	Measured with Br^- incubations (this study)
γ_{bi}	Irrigation scaling coefficient for O_2, TH_2S, Fe^{2+}	2, 2.5, 0	1	3-D and 1-D bioirrigation model (Meile et al., 2005)
γ_{bi}	Irrigation scaling coefficient for TPO_4	0.3	1	TPO_4 concentrations (this study)
γ_{bi}	Irrigation scaling coefficient for all other solutes	1	1	3-D and 1-D bioirrigation model (Meile et al., 2005)
α_{b1}	Coefficient for intracellular nitrate transport	Variable	d^{-1}	Steady state model (Dale et al., 2011) and TH_2S data
α_{b2}	Coefficient for intracellular nitrate transport	2	cm	*Beggiatoa* distributions (Preisler et al., 2007) and TH_2S data
α_{bu}	Bubble irrigation coefficient	Variable	d^{-1}	SO_4^{2-}, TCO_2 and NH_4^+ concentration profiles
z_{bu}	Depth affected by bubble irrigation	30	cm	SO_4^{2-}, TCO_2 and NH_4^+ concentration profiles
k_{H2Sox}	Rate constant for H_2S oxidation	2.7×10^4	$M^{-1}\,d^{-1}$	Compilation of rate constants (Dale et al., 2012)
k_{Fe2ox}	Rate constant for Fe^{2+} oxidation	2.7×10^5	$M^{-1}\,d^{-1}$	Compilation of rate constants (Dale et al., 2012)
k_{FeS2ox}	Rate constant for FeS_2 oxidation	2.7×10^3	$M^{-1}\,d^{-1}$	Dissolved Fe^{2+} data in winter (this study)
k_{FeS_2p}	Rate constant for FeS_2 precipitation	2.7×10^4	$M^{-1}\,d^{-1}$	Compilation of rate constants (Dale et al., 2012)
k_{Fe3red}	Rate constant for $Fe(OH)_3$ reduction	0.82	$cm^{1.5}\,mmol^{0.5}\,d^{-1}$	Namibian sediments inhabited by *Thiomargarita* (Dale et al., 2009a)
$K_{O_2'}^{Fe}$	Kinetic constant for $Fe(OH)_3$ reduction	2	μM	Constrained from Fe^{2+} concentration (this study)
ε	Molar P–Fe ratio for iron oxyhydroxides	0.1	$mol\,P\,(mol\,Fe)^{-1}$	Diagenetic modeling by Slomp et al. (1996)
$P:C$	Molar mineralization ratio of $P:C$ in POM	1/106	$mol\,P\,(mol\,C)^{-1}$	In situ fluxes and sediment profiles (Balzer et al., 1983; Balzer, 1984)

[a] Bottom water SO_4^{2-} and Br^- are scaled to salinity and shown in Fig. 2.

Title Page

Abstract | Introduction

Conclusions | References

Tables | Figures

◄ | ►

► |

Back | Close

Full Screen / Esc

Printer-friendly Version

Interactive Discussion

Table 4. Yearly integrated benthic sources and sinks of phosphate for the upper 40 cm in Boknis Eck (mmol m^{-2} yr^{-1}) listed from largest to smallest. Sources are positive and sinks are negative. Values have been rounded to the nearest integer.

Flux	Rate
Release by *Beggiatoa*	+137
Uptake by *Beggiatoa*	−137
Total flux to the water column	−92
Mineralization of organic P	+47
Dissolution of iron-bound P	+42
Dissolved flux from deeper sediments	+15
Co-precipitation with authigenic iron oxyhydroxides	−12
Σ	∼0
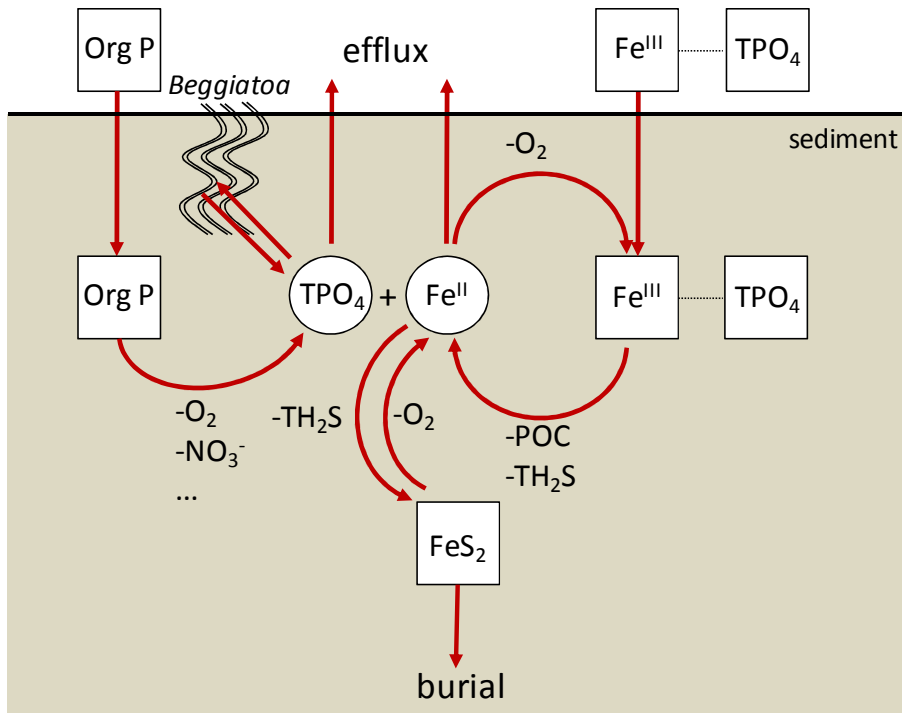
Fig. 1. Schematic of the coupled Fe and P cycles considered in the model. Solid species are in squares and solutes in circles. P is added to the sediment as organic P and with iron oxyhydroxides. Phosphate is released to the porewater upon reductive dissolution of ferric iron and oxidation of organic matter. This dissolved P pool is free to be transported out of the sediment, or removed from the porewater by co-precipitation with ferrous iron oxidation. P uptake and release by *Beggiatoa* is explored in Sect. 4.4.
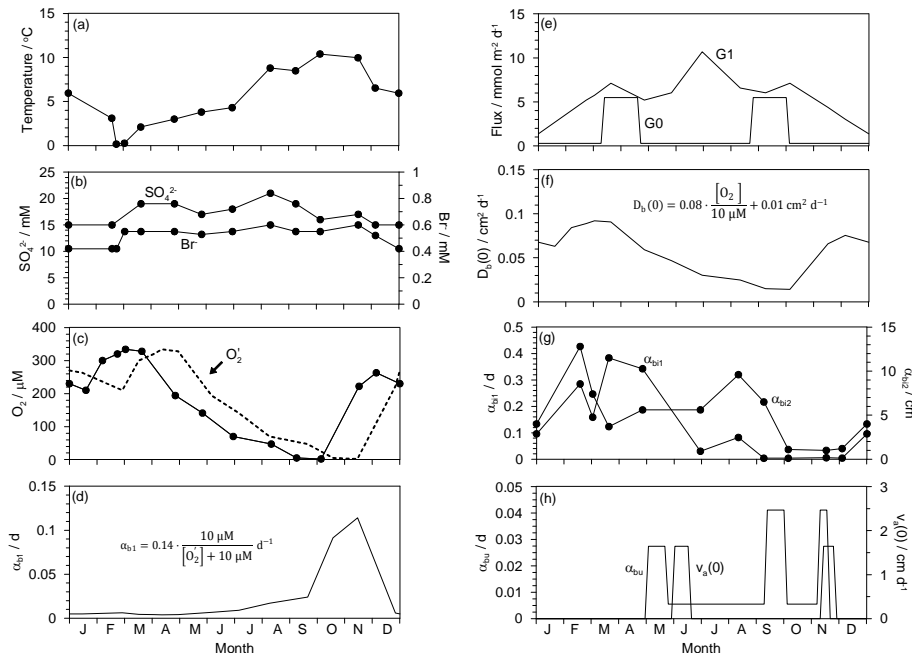
Fig. 2. Time-dependent boundary conditions and forcing functions used in the model. **(a)** Temperature, **(b)** bottom water sulfate and bromide, **(c)** bottom water dissolved oxygen and the time-lagged values (O_2') used to describe the rates of P uptake and release by *Beggiatoa*, $Fe(OH)_3$ reduction by sulfide and nitrate transport by sulfide oxidizing bacteria **(d)**. Panel **(e)** shows the G0 and G1 organic matter fluxes, **(f)** shows the bioturbation coefficient, **(g)** shows the bioirrigation coefficients (α_{bi1} and α_{bi2}), and **(h)** shows the bubble irrigation coefficient (α_{bu}) and enhanced advection of dissolved methane ($v_a(0)$). The symbols in **(a)**, **(b)**, **(c)** and **(g)** denote values that have been measured except from those at the beginning and the end of the year which are interpolated. Linear interpolations were used between the data for the modeling purposes. The rate of intracellular nitrate transport in **(d)** and bioturbation in **(f)** depend on oxygen concentrations according to the equations shown.

Discussion Paper | Discussion Paper | Discussion Paper | Discussion Paper

Title Page

Abstract | Introduction

Conclusions | References

Tables | Figures

|◄ | ►|

◄ | ►

Back | Close

Full Screen / Esc

Printer-friendly Version

Interactive Discussion
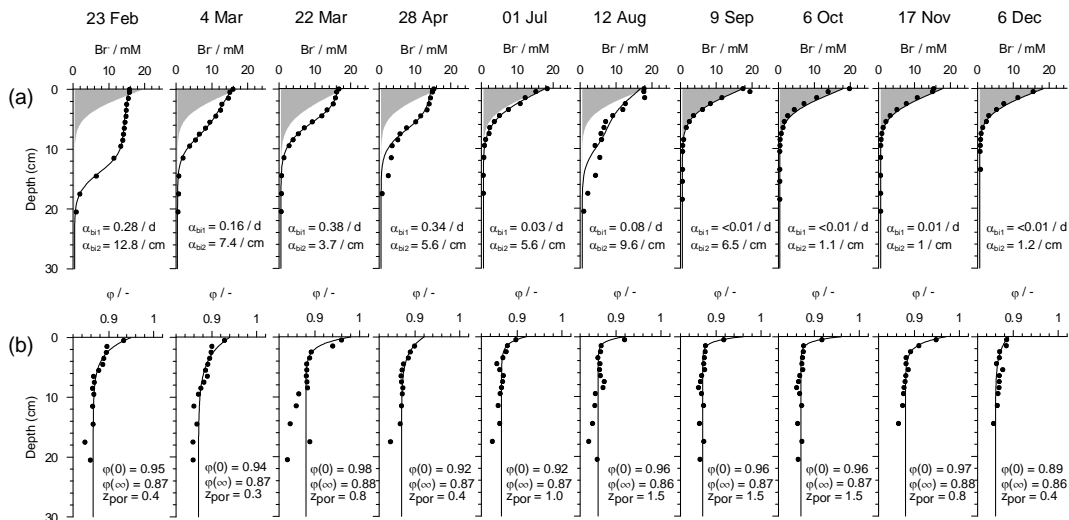
Fig. 3. (a) Bromide tracer concentrations (symbols) measured in cores incubated for bioirrigation experiments sampled on the day in 2010 indicated on the top of the figure. The curve represents the modeled tracer concentration at the end of the incubation period using the parameters indicated, and the shaded interval shows the expected bromide profile assuming transport by molecular diffusion only. For each model run, the modeled porosity curves shown in **(b)** were used, defined by the parameters indicated in each panel and the equation given in the text.
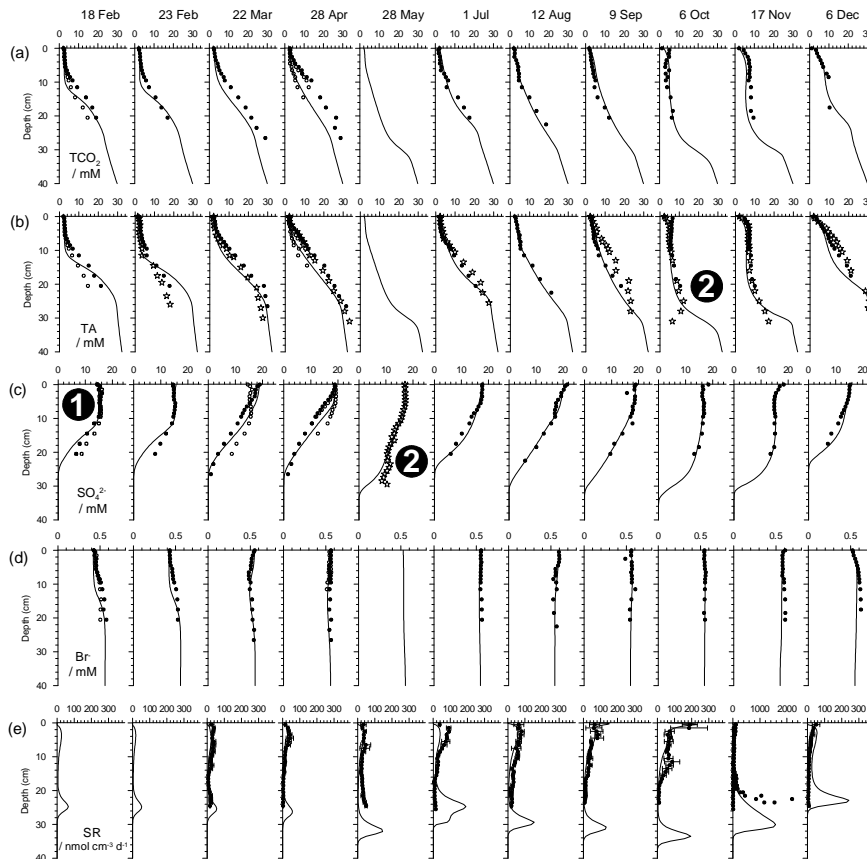
Fig. 4a. Simulated (curves) and measured (symbols) geochemical concentrations and SR rates in Boknis Eck sediments sampled on the dates indicated at the top of the figure. Open and closed circles indicate porewater measurements from adjacently sampled multi-cores sampled by squeezing the sediments. Stars indicate porewater extracted by rhizons. The error bars in **(e)** indicate the mean and standard deviation of 3 replicate SR rates sampled from the same core. SR rates in November are shown for the individual triplicate cores to highlight the very high rates measured in two of the sub-cores (note the change in scale). The modeled SR is the sum of sulfate consumption by organic carbon and methane oxidation ($0.5 \times R_{SO_4} + R_{AOM}$). The numbers 1 to 3 in black circles highlight examples of the salient seasonal features (1 = constant solute concentrations in the upper 10 cm in winter, 2 = shallowing of the concentration gradients in May and October/November, and 3 = the Fe^{2+} and TPO_4 peaks in winter and autumn.
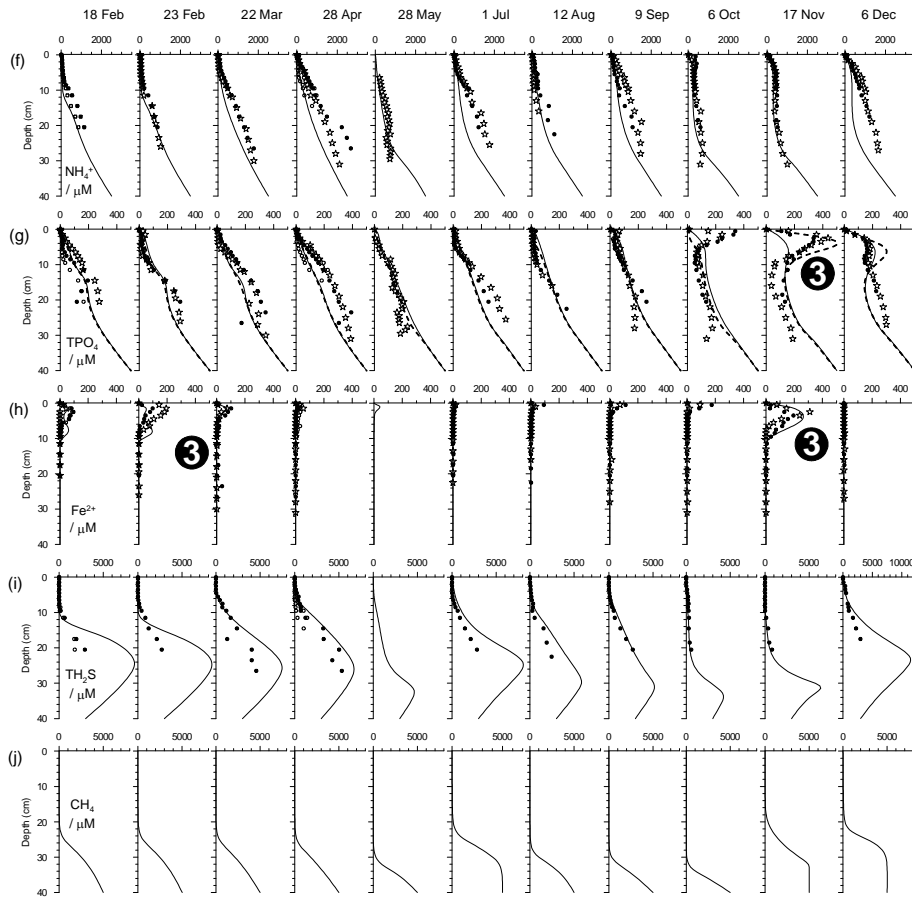
Benthic fluxes in seasonally-hypoxic sediments

A. W. Dale et al.

Title Page

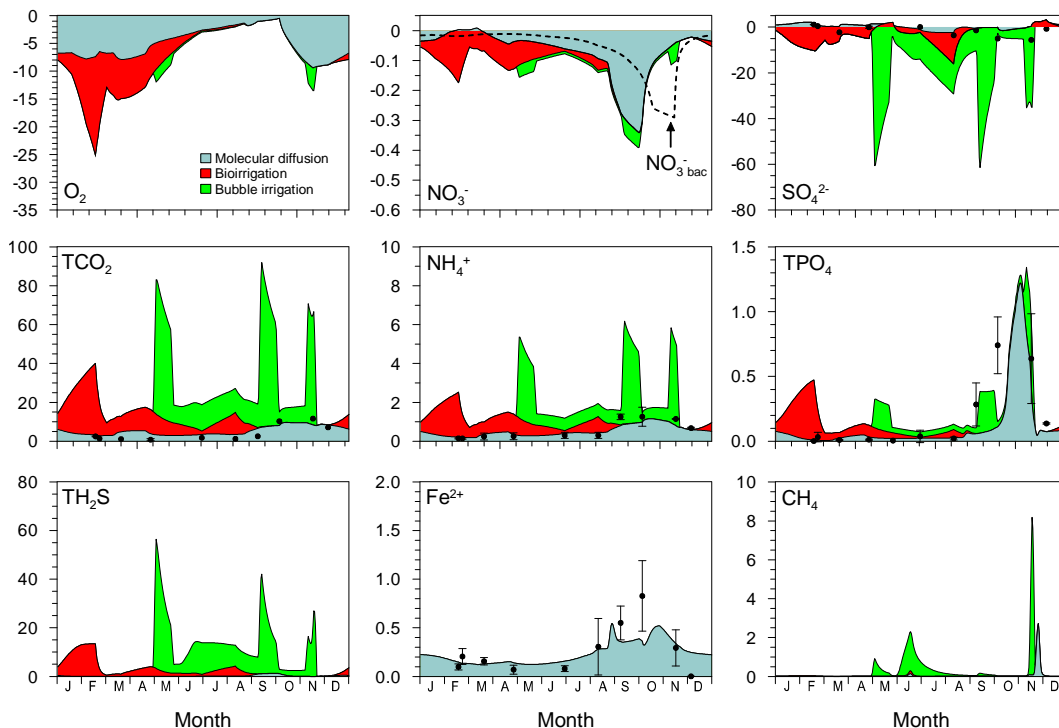| Abstract | Introduction |
| Conclusions | References |
| Tables | Figures |

Back | Close

Full Screen / Esc

Printer-friendly Version

Interactive Discussion

Fig. 4b. Continued.

Fig. 5. Modeled solute fluxes across the sediment water interface ($\mathrm{mmol\,m^{-2}\,d^{-1}}$) by molecular diffusion, bioirrigation and bubble irrigation. The black circles denote the mean ($\pm 1\sigma$) diffusive fluxes calculated by applying Fick's Law to the measured data. The dashed line in the NO_3^- plot denotes intracellular nitrate transport by *Beggiatoa*. Negative fluxes are into the sediment. Modeled phosphate fluxes correspond to the simulation considering P uptake and release by *Beggiatoa* (see text).

Title Page

Abstract | Introduction

Conclusions | References

Tables | Figures

|◄ | ►|

◄ | ►

Back | Close

Full Screen / Esc

Printer-friendly Version

Interactive Discussion
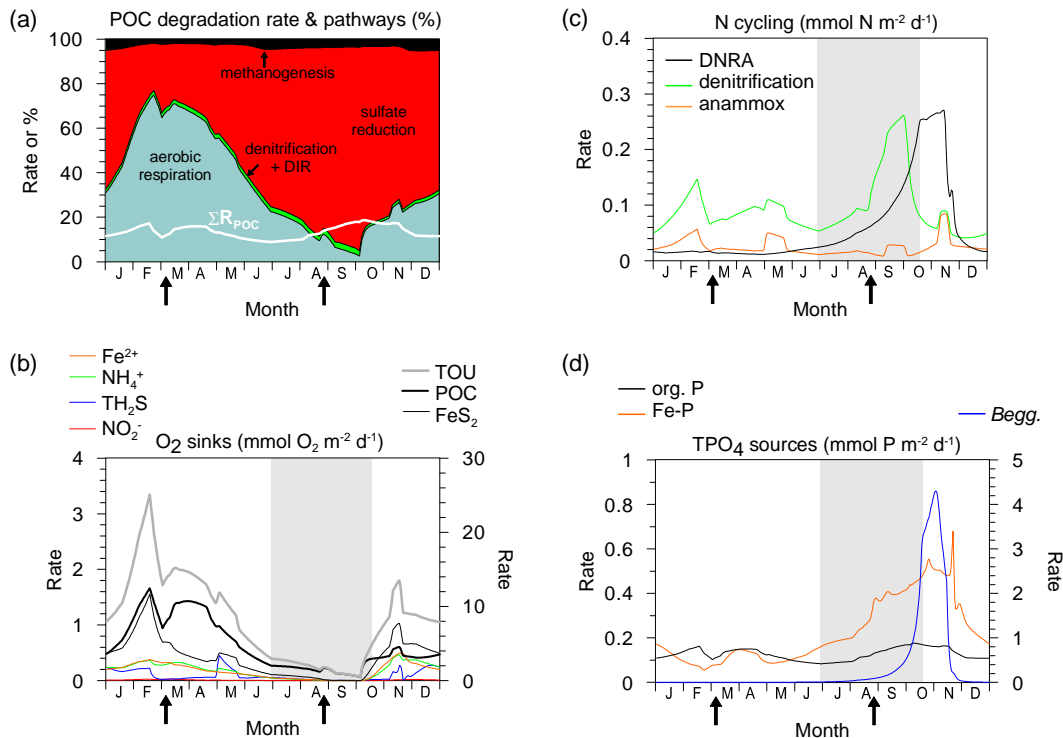
Fig. 6. (a) The daily fraction (%) of POM which is mineralized by each diagenetic pathway and the total rate of POM mineralization (ΣR_{POC} in $mmol\,m^{-2}\,d^{-1}$ of C shown by the white line). **(b)** Pathways of O_2 consumption ($mmol\,m^{-2}\,d^{-1}$ of O_2), **(c)** selected N cycling pathways ($mmol\,m^{-2}\,d^{-1}$ of N) and **(d)** biogeochemical reactions producing TPO_4 in the sediment ($mmol\,m^{-2}\,d^{-1}$ of TPO_4). The period with hypoxic bottom water ($O_2 < 63\,\mu M$) is indicated with the grey shaded area and the black arrows indicate the start of the spring and autumn blooms.
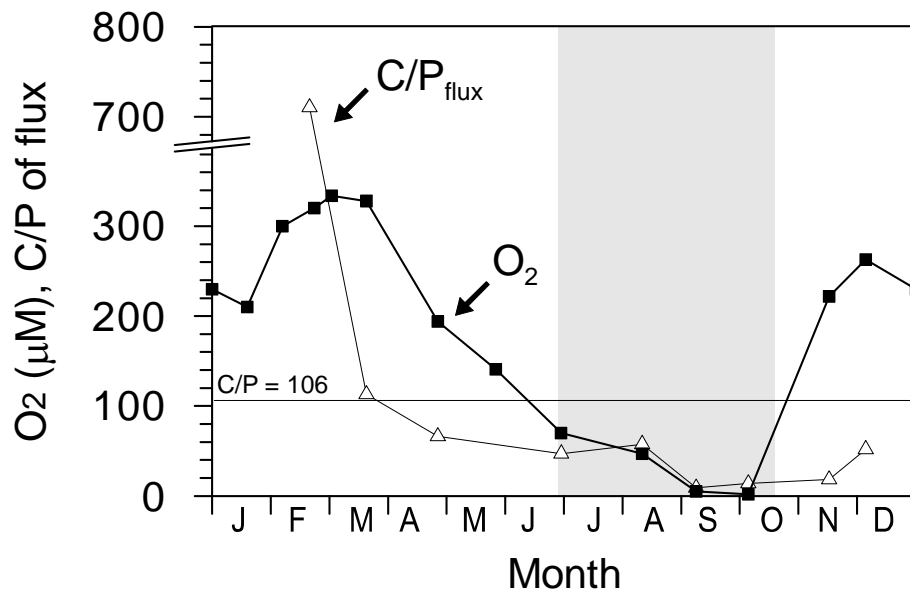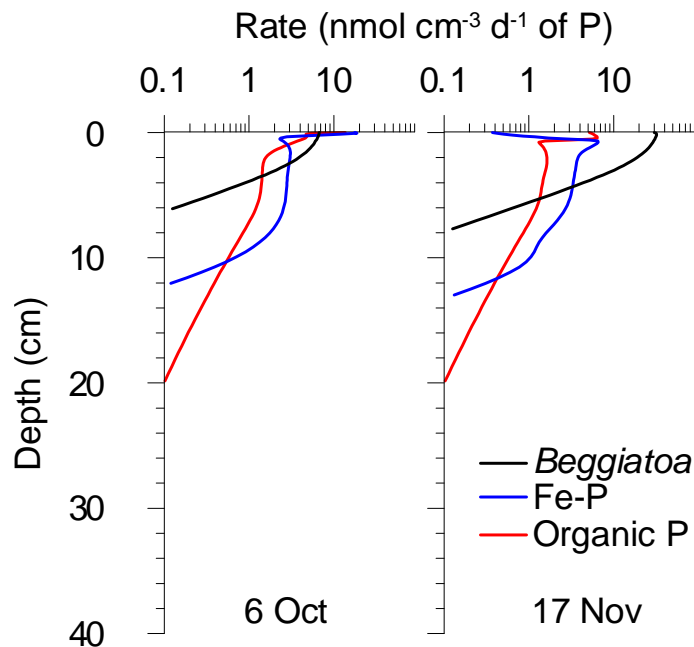
Fig. 7. Oxygen concentrations (from Fig. 2c) and the stoichiometry of the TCO_2 to TPO_4 flux (C/P) by molecular diffusion at the sediment-water interface calculated using the monthly measured data. The horizontal black line is the Redfield C/P ratio. Note the axis break in the ordinate.

Full Screen / Esc

Printer-friendly Version

Interactive Discussion

Fig. 8. Rates ($nmol\,cm^{-3}\,d^{-1}$ of P) of phosphate release from organic P, iron-bound P and sulfide oxidizing bacteria during October and November when large peaks in porewater TPO_4 were observed.